Supplementary Information (SI) for Physical Chemistry Chemical Physics.
This journal is © the Owner Societies 2025

Supporting Information: Photoinduced Decarboxylation in Fluorescent Proteins: Charge-Transfer States and Structure-Function Relationship

Janko Čivić,*,† Hideaki Mizuno,*,‡ and Jeremy N. Harvey*,†

†*Department of Chemistry, KU Leuven - Celestijnenlaan 200F, 3001 Leuven, Belgium*

‡*Department of Chemistry, KU Leuven - Celestijnenlaan 200G, 3001 Leuven, Belgium*

E-mail: janko.civic@kuleuven.be; hideaki.mizuno@kuleuven.be; jeremy.harvey@kuleuven.be

Table of Contents

System Preparation

Table S1: Equilibration protocol used to generate QM/MM optimized structures of PA-GFP, EGFP, DsRed, LSSmOrange, LSSmKate1, and PSLSSmKate.

Run	Calculation type	Restraints [kcal/mol Å^2]	Constant	Minimization steps / Simulation time	PBC	Timestep [fs]
1	minimization (CPU)	non-solvent 500	V	1000 steps	Yes	-
2	minimization (GPU)	CRO region 500	V	10 000 steps	Yes	-
3	heating (GPU) 0-300 K	CRO region 500	V	20 ps	Yes	2
4	equilibration (GPU)	CRO region 500	P	1 ns	Yes	2
5	cooling (GPU) 300-50 K	CRO region 500	V	20 ps	Yes	2
6	minimization (GPU)	CRO region 500	V	10 000 steps	Yes	-
7	QM/MM minimization (CPU)	border 1000	V	max 1000 steps	No	-

Table S2: Composition of the QM region for each fluorescent protein variant during QM/MM structure optimization. Residue numbering follows the original PDB files.

Variant	Residues included in the QM region
PA-GFP	chromophore, Phe64 (backbone C, O), Val68 (backbone N, H, CA, HA); water: 241, 383, 253; side chain: Glu222, His148, Ser205, Arg96, Gln94
EGFP	chromophore, Leu64 (backbone C, O), Val68 (backbone N, H, CA, HA); water: 2084, 2259; side chain: Glu222, His148, Thr203, Ser205, Arg96, Gln94
DsRed	chromophore, Phe65 (backbone C, O, CA, HA), Ser69 (backbone N, H, CA, HA); water: 236, 238; side chain: Glu215, Lys163, Ser146, Arg95, Lys70
LSSmOrange	chromophore, Gln64 (backbone C, O, CA, HA), Ser69 (backbone N, H, CA, HA); water: 456; side chain: Glu215, Asp161, Ser146, Arg95, Lys70
LSSmKate1	chromophore, Phe62 (backbone C, O, CA, HA), Ser66 (backbone N, H, CA, HA); water: 249; side chain: Glu215, Glu160, Arg197, Arg92
PSLSSmKate	chromophore, Phe62 (backbone C, O, CA, HA), Ser66 (backbone N, H, CA, HA); water: 319; side chain: Glu215, Glu160, Ser143, Arg92, Arg197

Table S3: Composition of the QM region used in QM/MM excited-state calculations for each fluorescent protein variant. Amino acid residue numbering follows the original PDB files, while water molecule indices correspond to the prepared systems. Residues were capped with hydrogen, carbonyl, or amine groups where required.

Variant	Residues included in the QM region
PA-GFP (1)	**complete**: chromophore; **side chain**: Glu222
PA-GFP (2)	**complete**: chromophore, Glu222, Wat313; **side chain**: Ser205
PA-GFP (3)	**complete**: chromophore, Glu222, Wat313, Wat306; **side chain**: Ser205, Arg96, Gln94
PA-GFP (4)	**complete**: chromophore, Glu222, Thr62, Wat313, Wat306, Wat309; **side chain**: Ser205, Arg96, Gln94, Gln69, Tyr145, His148, His203
EGFP	**complete**: chromophore, Glu222, Wat306, Wat295; **side chain**: Gln94, Arg96, His148, Thr203
LSSmOrange	**complete**: chromophore, Glu215, Wat305, Wat306, Wat307; **side chain**: Ser146, Arg95, Lys70, Gln42
DsRed	**complete**: chromophore, Glu215, Wat278, Wat279, Wat288; **side chain**: Lys163, Ser146, Arg95, Lys70, Asn42; **backbone**: Phe65
LSSmKate1	**complete**: chromophore, Glu215, Wat297, Wat300, Wat309, Wat313; **side chain**: Glu160, Arg197, Arg92, Gln39; **backbone**: Phe62
PSLSSmKate (P1)	**complete**: chromophore, Glu215, Wat297, Wat299, Wat301, Wat303; **side chain**: Glu160, Arg92, Arg197; **backbone**: Phe62
PSLSSmKate (P2)	**complete**: chromophore, Glu215, Wat296, Wat298, Wat8074; **side chain**: Glu160, Arg92, Arg197; **backbone**: Phe62

P1 - deprotonated Glu215, P2 - neutral Glu215

PA-GFP Benchmark Study

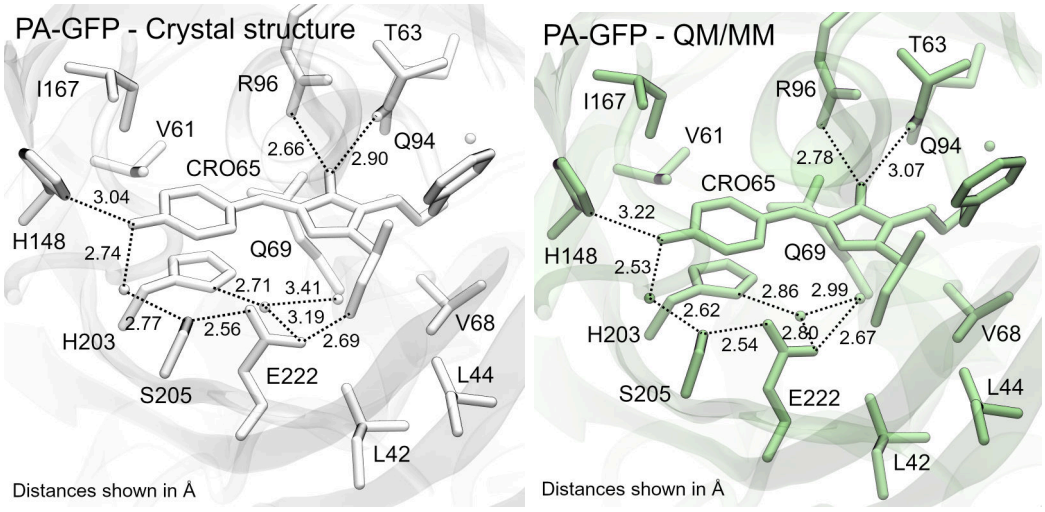

Figure S1: Comparison of H-bond networks in QM/MM optimized (green) and crystal (white, PDB: 3GJ1[1]) structures of PA-GFP. The chromophore and nearby amino acid residues are shown as sticks and nearby water molecules as spheres. Hydrogen atoms are omitted for clarity.

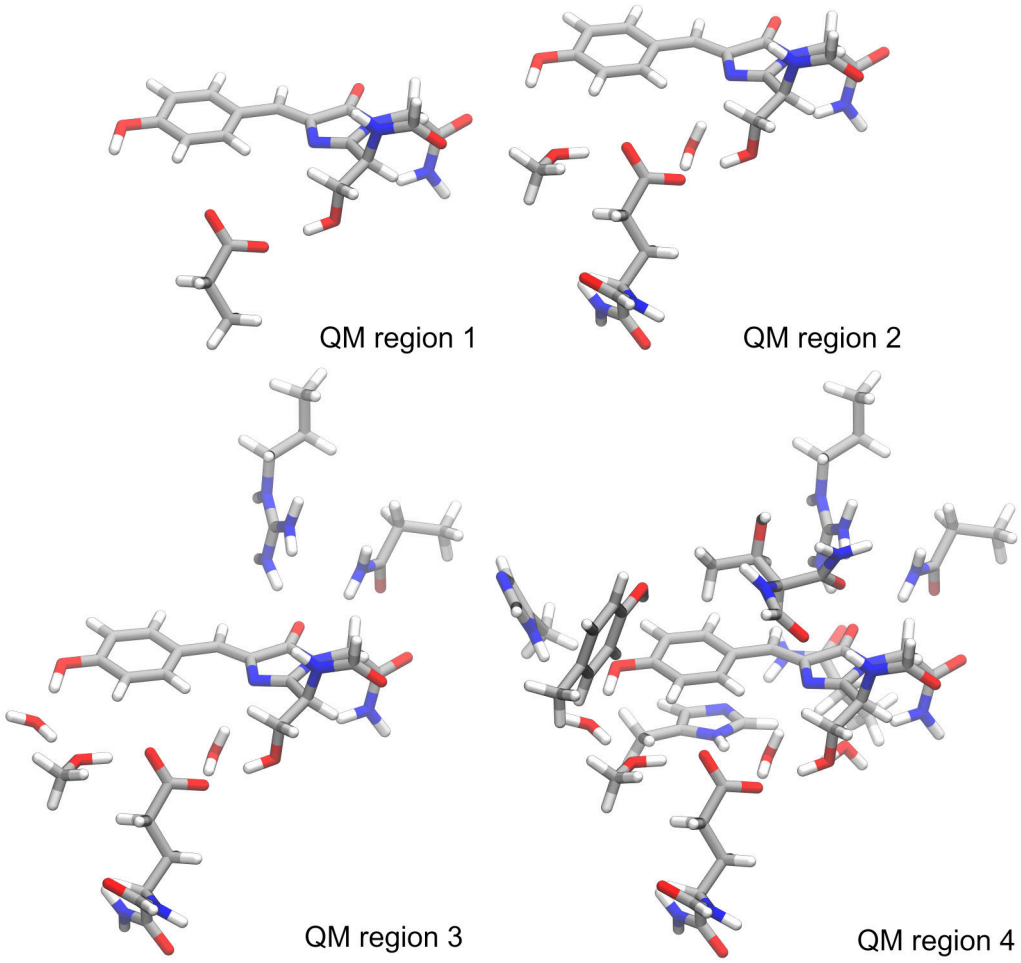

Figure S2: QM regions used in excited-state QM/MM calculations of PA-GFP. The rest of the system, not shown here, was described with electrostatic or polarizable embedding.

Table S4: Energies of the first excited state and the Glu222–chromophore charge transfer states in PA-GFP, computed using various approaches. The composition of the QM regions is described in Table S3.

QM Region	Embedding	Method	Basis set	S_1 / eV	CT (Glu222-Cro) / eV
1	EE	CAM-B3LYP (D3-BJ)	def2-TZVP	3.50	4.10, 4.17, 4.45
			def2-TZVPD	3.46	4.14, 4.20, 4.53
		wB97X-D	def2-TZVP	3.51	4.28, 4.32, 4.38, 4.67
			def2-TZVPD	3.48	4.32, 4.33, 4.40, 4.71
		CC2	def2-TZVP	3.34	3.89, 3.95, 4.46
			RVS(core)-def2-TZVP	3.34	3.89, 3.96, 4.47
			RVS(600 eV)-def2-TZVP	3.34	3.89, 3.96, 4.47
			RVS(200 eV)-def2-TZVP	3.34	3.86, 3.93, 4.45
			RVS(160 eV)-def2-TZVP	3.33	3.79, 3.88, 4.38
			RVS(140 eV)-def2-TZVP	3.33	3.77, 3.87, 4.37
			RVS(120 eV)-def2-TZVP	3.33	3.78, 3.86, 4.37
			RVS(100 eV)-def2-TZVP	3.34	3.74, 3.84, 4.39
			RVS(90 eV)-def2-TZVP	3.35	3.80, 3.89, 4.42
			RVS(80 eV)-def2-TZVP	3.36	3.88, 3.95, 4.40
			RVS(70 eV)-def2-TZVP	3.36	3.89, 3.95, 4.42
			RVS(60 eV) def2-TZVP	3.37	3.91, 3.96, 4.44
		ADC(2)	def2-TZVP	3.21	3.76, 3.87, 4.33
			RVS(core)-def2-TZVP	3.22	3.77, 3.88, 4.34
			RVS(600 eV)-def2-TZVP	3.22	3.77, 3.88, 4.34
			RVS(200 eV)-def2-TZVP	3.21	3.71, 3.83, 4.30
			RVS(160 eV)-def2-TZVP	3.19	3.58, 3.73, 4.15
			RVS(140 eV)-def2-TZVP	3.19	3.56, 3.72, 4.14
			RVS(120 eV)-def2-TZVP	3.19	3.57, 3.72, 4.14
			RVS(100 eV)-def2-TZVP	3.19	3.51, 3.68, 4.15
			RVS(90 eV)-def2-TZVP	3.21	3.55, 3.70, 4.17
			RVS(80 eV)-def2-TZVP	3.21	3.62, 3.75, 4.13
			RVS(70 eV)-def2-TZVP	3.21	3.62, 3.76, 4.15
			RVS(60 eV)-def2-TZVP	3.22	3.63, 3.77, 4.16
	PE	CAM-B3LYP (D3-BJ)	def2-TZVP	3.42	5.48, 5.97, 6.16
			def2-TZVPD	3.37	-
		wB97X-D	def2-TZVP	3.44	5.83, 6.16, 6.36
			def2-TZVPD	3.39	-
		CC2	def2-TZVP	3.27	5.32
			RVS(60 eV)-def2-TZVP	3.30	5.34
		ADC(2)	def2-TZVP	3.20	5.25
			RVS(60 eV)-def2-TZVP	3.20	5.14
2	EE	CAM-B3LYP (D3-BJ)	def2-TZVP	3.48	4.81, 4.94, 5.24, 5.37
			def2-TZVPD	3.45	4.83, 4.95, 5.25, 5.38
		wB97X-D	def2-TZVP	3.50	5.00, 5.11, 5.52
			def2-TZVPD	3.47	5.02, 5.12, 5.54
		CC2	def2-TZVP	3.32	4.40, 4.53, 5.08
			RVS(60 eV)-def2-TZVP	3.35	4.39, 4.54, 5.03
		ADC(2)	def2-TZVP	3.19	4.28, 4.45, 4.95
			RVS(60 eV)-def2-TZVP	3.20	4.12, 4.34, 4.78
	PE	CAM-B3LYP (D3-BJ)	def2-TZVP	3.42	5.04, 5.10, 5.60
			def2-TZVPD	3.37	5.06
		wB97X-D	def2-TZVP	3.44	5.26, 5.35, 5.79
			def2-TZVPD	3.40	5.29
		CC2	RVS(60 eV)-def2-TZVP	3.31	4.68, 4.72, 5.39
		ADC(2)	RVS(60 eV)-def2-TZVP	3.21	4.43, 4.52, 5.12
3	EE	CAM-B3LYP (D3-BJ)	def2-TZVP	3.38	4.91, 4.99, 5.42
			def2-TZVPD	3.36	4.93, 5.00, 5.43
		wB97X-D	def2-TZVP	3.40	5.09, 5.15, 5.58
			def2-TZVPD	3.38	5.10, 5.16, 5.59
		CC2	RVS(60 eV)-def2-TZVP	3.18	4.41, 4.53, 5.04
		ADC(2)	RVS(60 eV)-def2-TZVP	3.02	4.14, 4.33, 4.79
	PE	CAM-B3LYP (D3-BJ)	def2-TZVP	3.43	5.08, 5.13, 5.23, 5.65
			def2-TZVPD	3.40	5.12
		wB97X-D	def2-TZVP	3.44	5.30, 5.37, 5.83
			def2-TZVPD	3.42	5.33
		CC2	RVS(60 eV)-def2-TZVP	3.31	4.69, 4.69, 5.39
		ADC(2)	RVS(60 eV)-def2-TZVP	3.21	4.42, 4.51, 5.13
	PE (10 Å cutoff)	CAM-B3LYP (D3-BJ)	def2-TZVP	3.38	5.20, 5.24, 5.73
4	EE	CAM-B3LYP (D3-BJ)	def2-TZVP	3.32	5.03
		wB97X-D	def2-TZVP	3.35	5.12, 5.18, 5.62
	PE	CAM-B3LYP (D3-BJ)	def2-TZVP	3.38	5.05, 5.07, 5.17, 5.59
		wB97X-D	def2-TZVP	3.40	5.24, 5.31, 5.77

Table S5: Energies of the first excited state and the Glu222–chromophore charge transfer states in the PA-GFP model, computed using CC2/def2-TZVP and ADC(2)/def2-TZVP, with and without the RVS approximation (excluding virtual orbitals above 60 eV). The composition of the QM regions is described in Table S3.

Method	QM Region	Embedding	RVS	S_1 [eV]	CT_1 [eV]	CT_2 [eV]	CT_3 [eV]
CC2	1	Electrostatic	full	3.340	3.886	3.950	4.462
			> 60 eV	3.371	3.908	3.963	4.437
		Polarizable	full	3.269	5.319	-	-
			> 60 eV	3.299	5.345	-	-
	2	Electrostatic	full	3.316	4.401	4.529	5.075
			> 60 eV	3.349	4.387	4.535	5.029
ADC(2)	1	Electrostatic	full	3.213	3.759	3.870	4.333
			> 60 eV	3.221	3.631	3.765	4.164
		Polarizable	full	3.199	5.246	-	-
			> 60 eV	3.204	5.142	-	-
	2	Electrostatic	full	3.189	4.280	4.453	4.945
			> 60 eV	3.197	4.119	4.339	4.777

Table S6: Energies of the first excited state and the Glu222-chromophore charge transfer states in the PA-GFP model with the smallest quantum region (Table S3) and electrostatic embedding, calculated using RVS-ADC(2)/def2-TZVP with varying energy cutoffs for discarding virtual orbitals. The total number of orbitals is 1025.

Discarded orbitals	% Discarded	S_1 [eV]	CT_1 [eV]	CT_2 [eV]	CT_3 [eV]
full	0	3.213	3.759	3.870	4.333
core	2.8	3.217	3.767	3.877	4.340
> 600 eV	5.7	3.217	3.767	3.877	4.340
> 200 eV	7.2	3.213	3.709	3.827	4.304
> 160 eV	14	3.191	3.575	3.731	4.148
> 140 eV	20	3.187	3.564	3.722	4.136
> 120 eV	25	3.187	3.571	3.720	4.144
> 100 eV	34	3.193	3.511	3.681	4.150
> 90 eV	40	3.206	3.550	3.704	4.167
> 80 eV	46	3.209	3.615	3.751	4.128
> 70 eV	51	3.214	3.617	3.756	4.148
> 60 eV	56	3.221	3.631	3.765	4.164

Table S7: Impact of the RVS approximation on the first excited state and the Glu222-chromophore charge transfer states in the PA-GFP model with the smallest quantum region (Table S3) and electrostatic embedding, calculated using RVS-CC2/def2-TZVP with varying energy cutoffs for discarding virtual orbitals. The total number of orbitals is 1025.

Discarded orbitals	% Discarded	S_1 [eV]	CT_1 [eV]	CT_2 [eV]	CT_3 [eV]
full	0	3.340	3.886	3.950	4.462
core	2.8	3.342	3.893	3.957	4.468
$>$ 600 eV	5.7	3.342	3.893	3.957	4.468
$>$ 200 eV	7.2	3.341	3.864	3.929	4.448
$>$ 160 eV	14	3.332	3.786	3.877	4.381
$>$ 140 eV	20	3.332	3.774	3.867	4.368
$>$ 120 eV	25	3.332	3.782	3.864	4.373
$>$ 100 eV	34	3.338	3.742	3.843	4.393
$>$ 90 eV	40	3.348	3.802	3.886	4.422
$>$ 80 eV	46	3.357	3.885	3.947	4.404
$>$ 70 eV	51	3.364	3.892	3.952	4.421
$>$ 60 eV	56	3.371	3.908	3.963	4.437

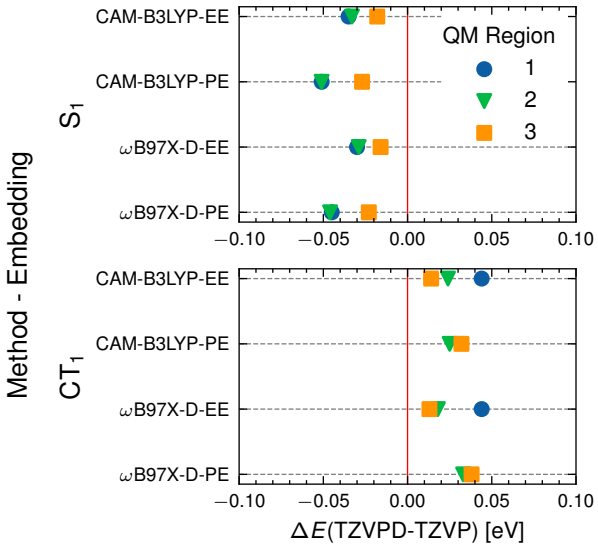

Figure S3: Impact of increasing basis set size on the first excited state and the first Glu222-chromophore charge transfer state in PA-GFP, calculated using different methods, embedding types and QM region sizes. The composition of the QM regions is described in Table S3.

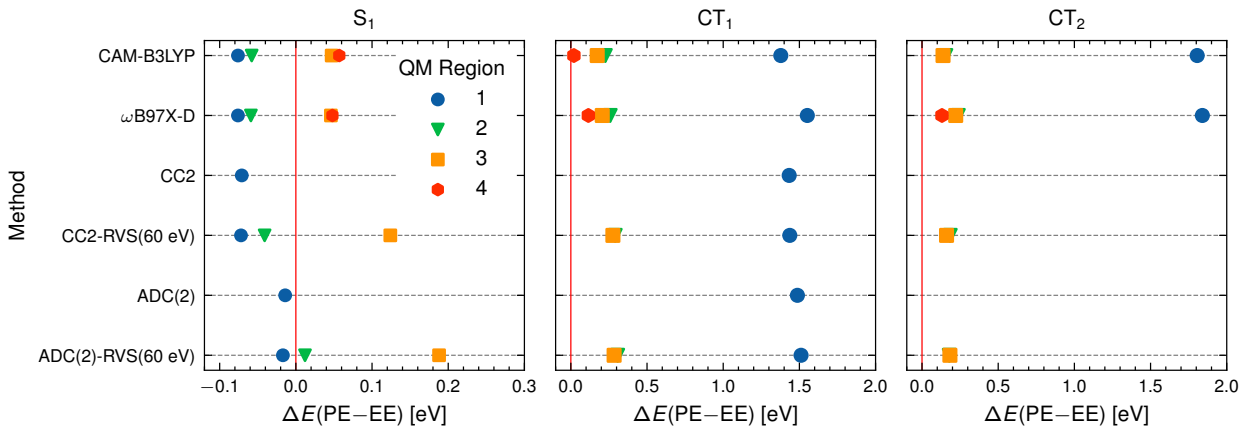

Figure S4: Impact of polarizable (PE) over electrostatic embedding (EE) on the first excited state and the first two Glu222-chromophore charge transfer states in PA-GFP, calculated with def2-TZVP using different methods and QM region sizes. The composition of the QM regions is described in Table S3.

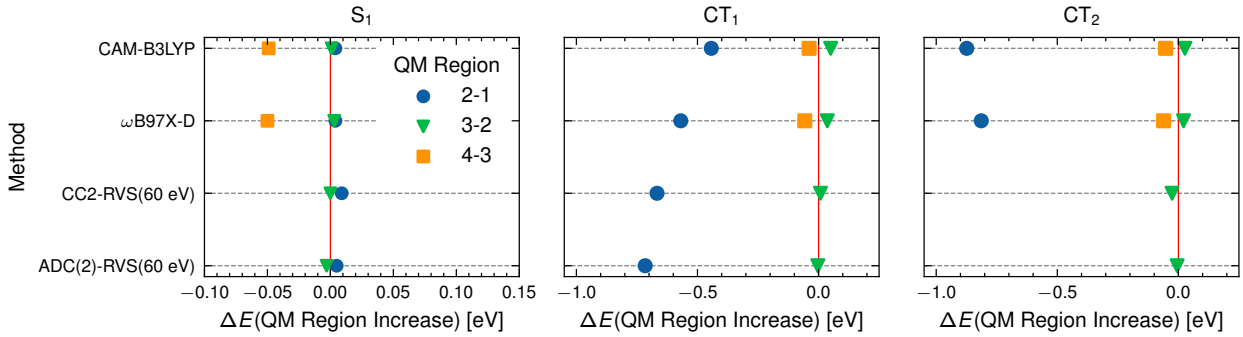

Figure S5: Impact of increasing the QM region on the first excited state and the first two Glu222-chromophore charge transfer states in PA-GFP, calculated with def2-TZVP and polarizable embedding. The composition of the QM regions is described in Table S3.

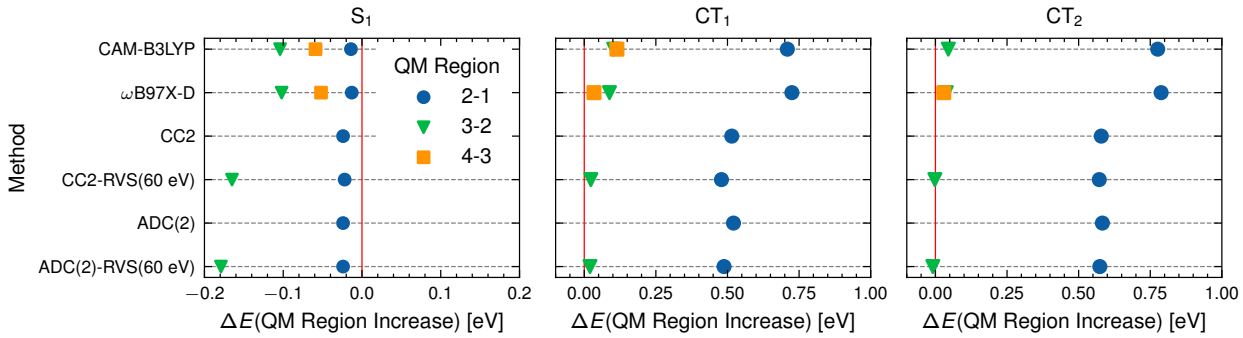

Figure S6: Impact of increasing the QM region on the first excited state and the first two Glu222-chromophore charge transfer states in PA-GFP, calculated with def2-TZVP and electrostatic embedding. The composition of the QM regions is described in Table S3.

State	$\Delta E(S_0 \rightarrow S_n)$/eV	f
1	3.426	1.017
2	4.383	0.002
3	4.643	0.004
4	4.747	0.017
5	5.085	0.001
6	5.126	0.001
7	5.234	0.004
8	5.366	0.189
9	5.608	0.061
10	5.648	0.000
11	5.842	0.003
12	5.877	0.007
13	5.907	0.012
14	5.954	0.004
15	5.963	0.004

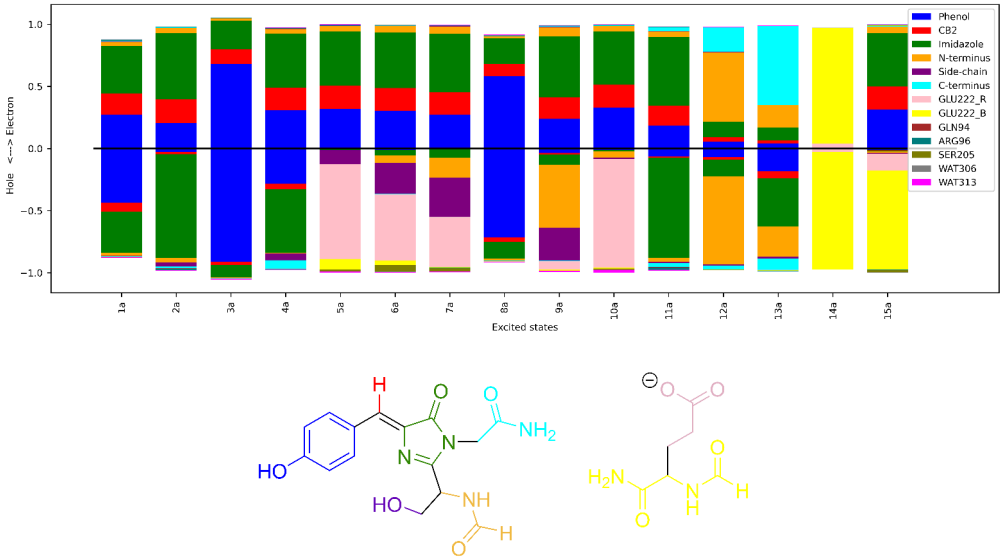

Figure S7: Fragment decomposition performed with TheoDORE of electron and hole populations of excited states of PA-GFP calculated with CAM-B3LYP/def2-TZVP with QM region 3 and polarizable embedding. Vertical excitation energies and oscillator strengths of each state are shown on the top. The fragments corresponding to the chromophore and Glu222 are shown below, with colors matching those used in the plot.

State	$\Delta E(S_0 \rightarrow S_n)$/eV	f
1	3.445	1.013
2	4.321	0.002
3	4.674	0.006
4	4.767	0.024
5	5.207	0.004
6	5.296	0.001
7	5.368	0.005
8	5.417	0.197
9	5.687	0.063
10	5.811	0.013
11	5.833	0.001
12	5.915	0.002
13	5.948	0.004
14	6.028	0.044
15	6.041	0.011

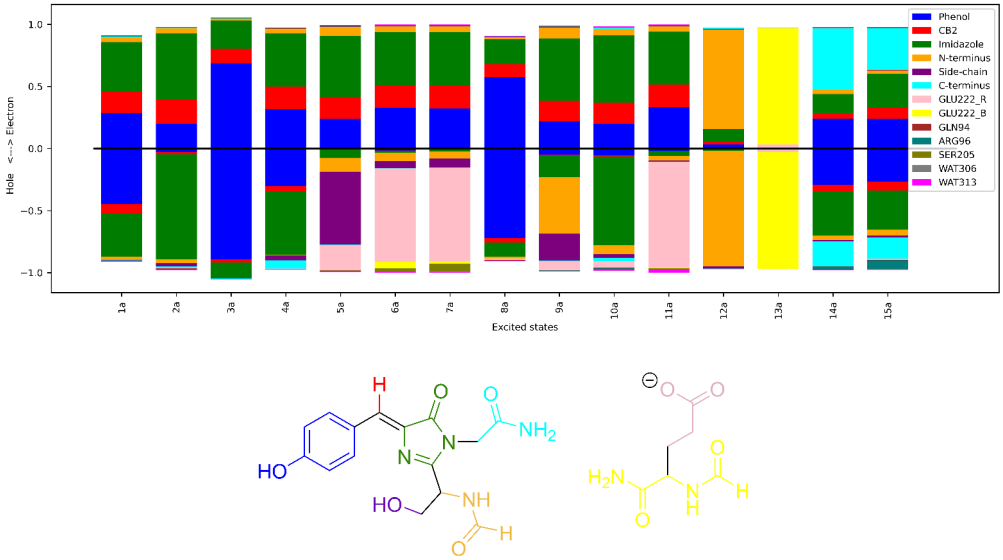

Figure S8: Fragment decomposition performed with TheoDORE of electron and hole populations of excited states of PA-GFP calculated with ωB97X-D/def2-TZVP with QM region 3 and polarizable embedding. Vertical excitation energies and oscillator strengths of each state are shown on the top. The fragments corresponding to the chromophore and Glu222 are shown below, with colors matching those used in the plot.

State	$\Delta E(S_0 \rightarrow S_n)$/eV	f
1	3.206	0.858
2	3.852	0.001
3	4.251	0.031
4	4.423	0.000
5	4.479	0.005
6	4.513	0.001
7	4.879	0.015
8	5.134	0.040
9	5.233	0.150
10	5.299	0.034

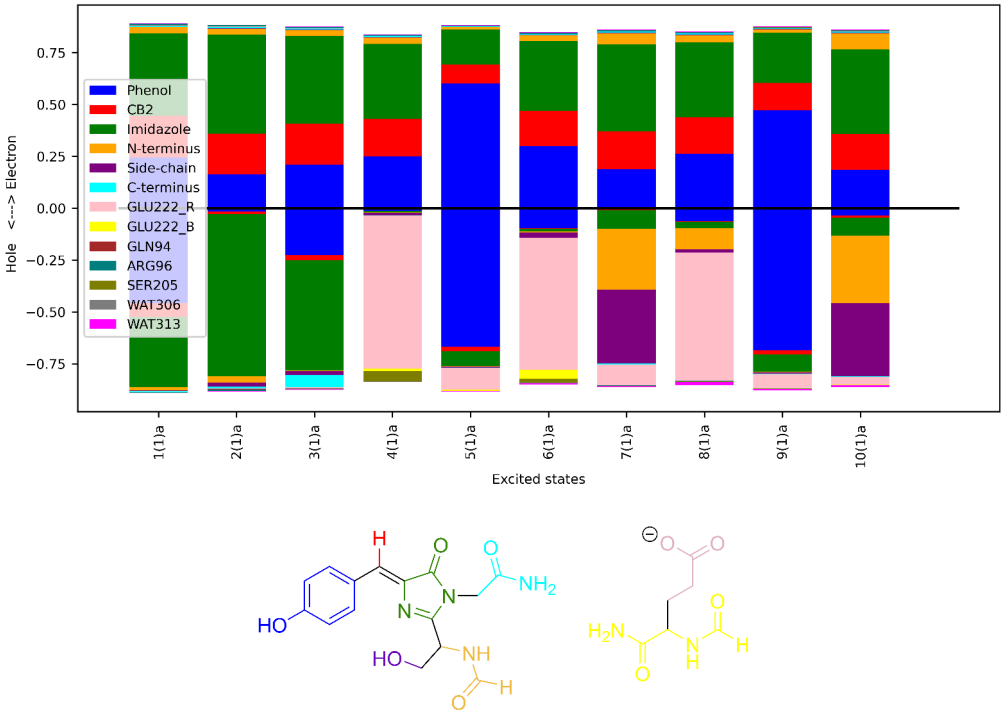

Figure S9: Fragment decomposition performed with TheoDORE of electron and hole populations of excited states of PA-GFP calculated with RVS-ADC(2)/def2-TZVP with QM region 3 and polarizable embedding. Vertical excitation energies and oscillator strengths of each state are shown on the top. The fragments corresponding to the chromophore and Glu222 are shown below, with colors matching those used in the plot.

State	$\Delta E(S_0 \rightarrow S_n)$/eV	f
1	3.308	1.089
2	4.073	0.002
3	4.380	0.026
4	4.513	0.002
5	4.686	0.000
6	4.694	0.000
7	5.065	0.031
8	5.233	0.180
9	5.393	0.005
10	5.497	0.071

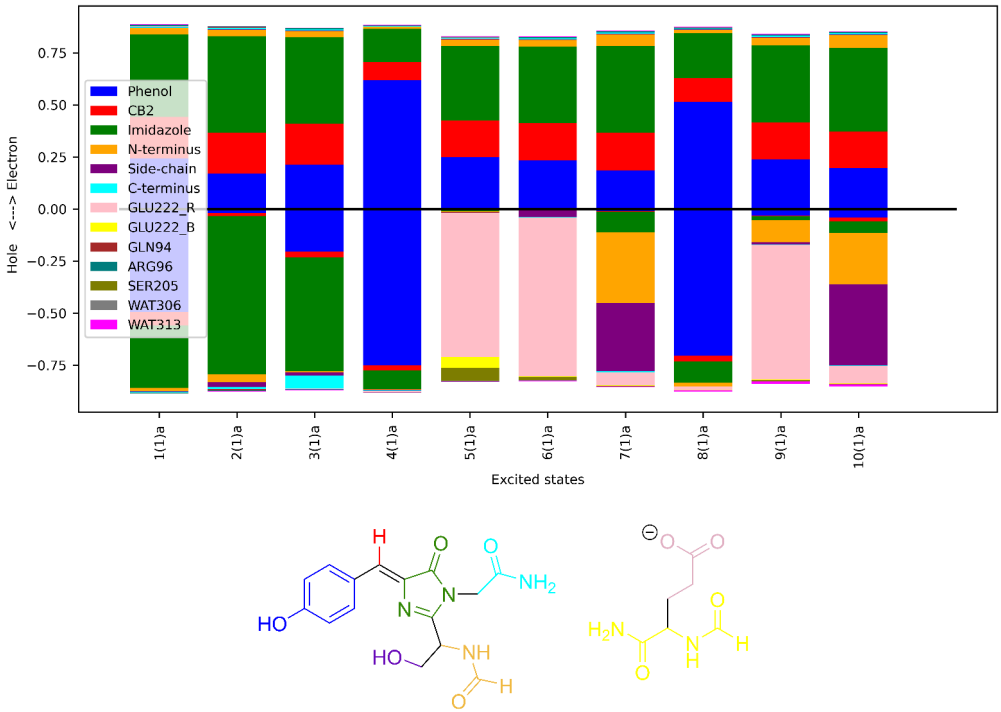

Figure S10: Fragment decomposition performed with TheoDORE of electron and hole populations of excited states of PA-GFP calculated with RVS-CC2/def2-TZVP with QM region 3 and polarizable embedding. Vertical excitation energies and oscillator strengths of each state are shown on the top. The fragments corresponding to the chromophore and Glu222 are shown below, with colors matching those used in the plot.

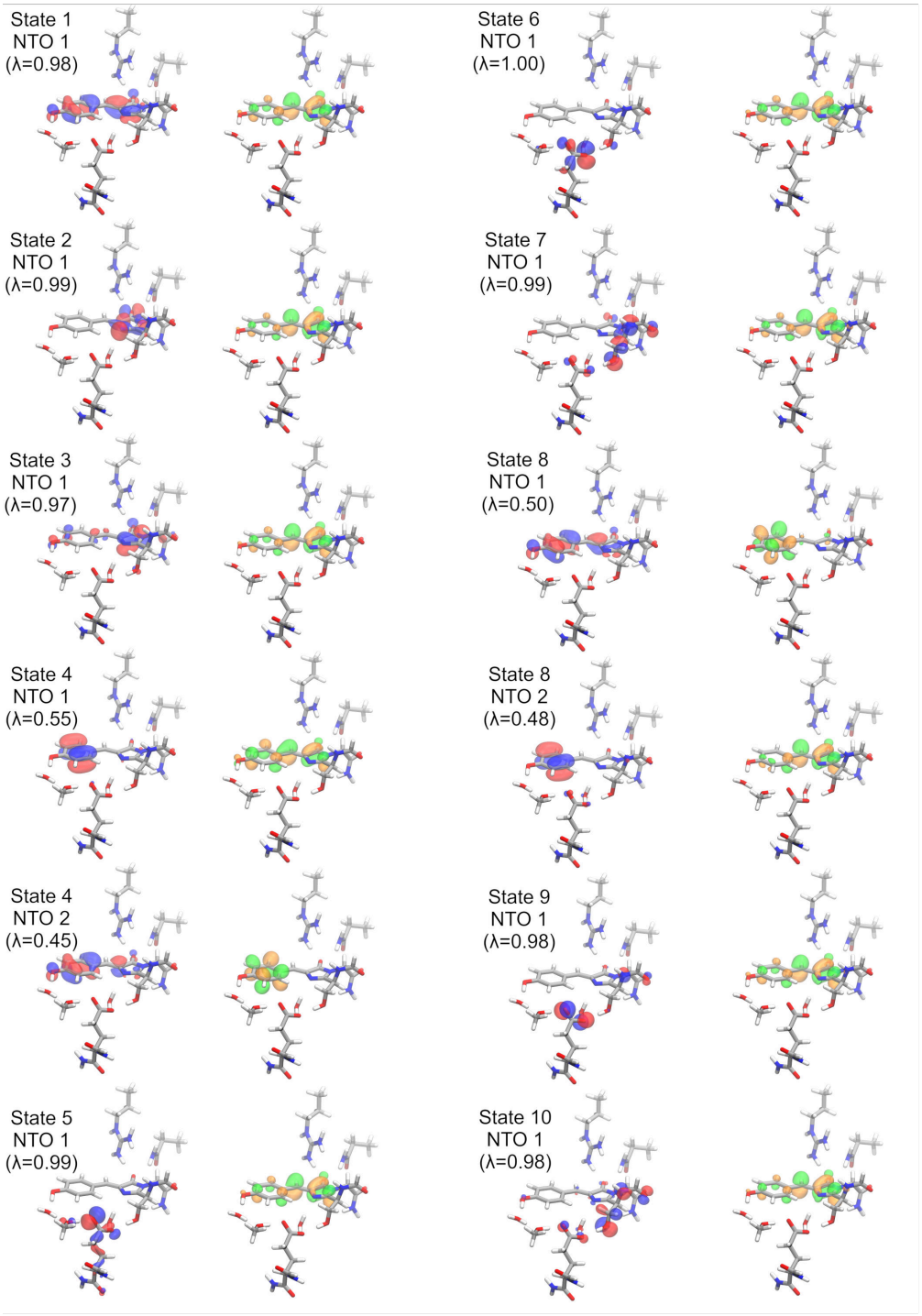

Figure S11: Most significant hole (red, blue) and electron (orange, green) NTOs of PA-GFP excited states, calculated with RVS-CC2/def2-TZVP, corresponding to Figure S10.

LSSmOrange

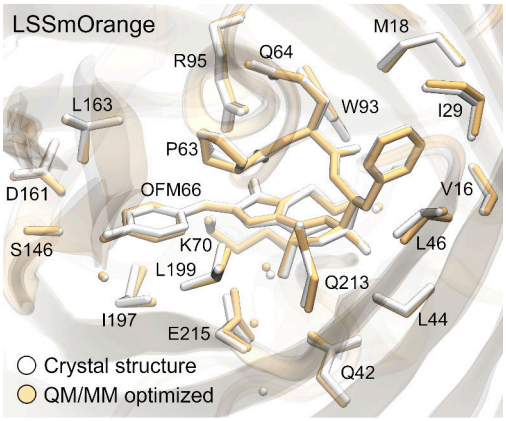

Figure S12: Comparison of QM/MM optimized (orange) and crystal (white, PDB: 4Q7R[2]) structure of LSSmOrange. The chromophore and nearby amino acid residues are shown as sticks and nearby water molecules as spheres. Hydrogen atoms are omitted for clarity.

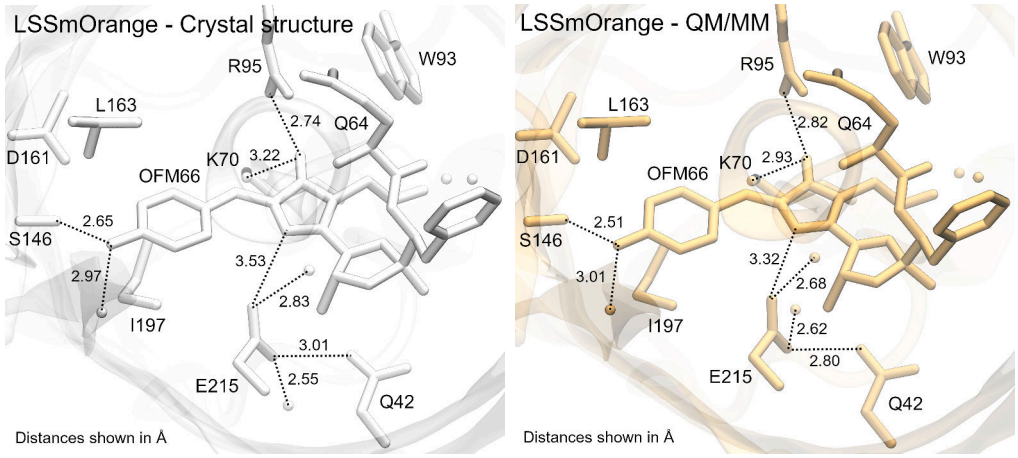

Figure S13: Comparison of H-bond networks in QM/MM optimized (orange) and crystal (white, PDB: 4Q7R[2]) structure of LSSmOrange. The chromophore and nearby amino acid residues are shown as sticks and nearby water molecules as spheres. Hydrogen atoms are omitted for clarity.

State	$\Delta E(S_0 \rightarrow S_n)$/eV	f
1	2.873	1.102
2	3.826	0.009
3	3.976	0.037
4	4.058	0.001
5	4.373	0.001
6	4.489	0.001
7	4.573	0.012
8	4.711	0.017
9	4.752	0.184
10	4.914	0.009

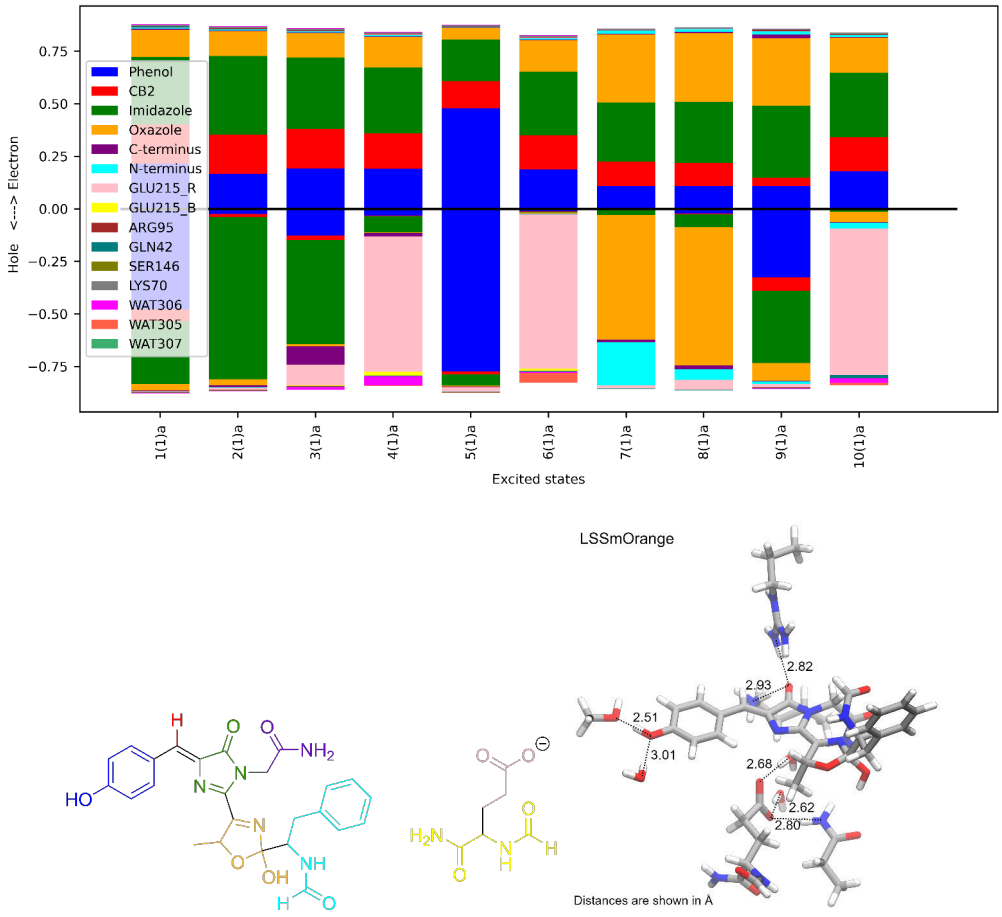

Figure S14: Fragment decomposition performed with TheoDORE of electron and hole populations of excited states of LSSmOrange calculated with CC2/def2-TZVP. Vertical excitation energies and oscillator strengths of each state are shown on the top. The QM region used in the excited-state calculations and fragments corresponding to the chromophore and Glu215 are shown below, with colors matching those used in the plot.

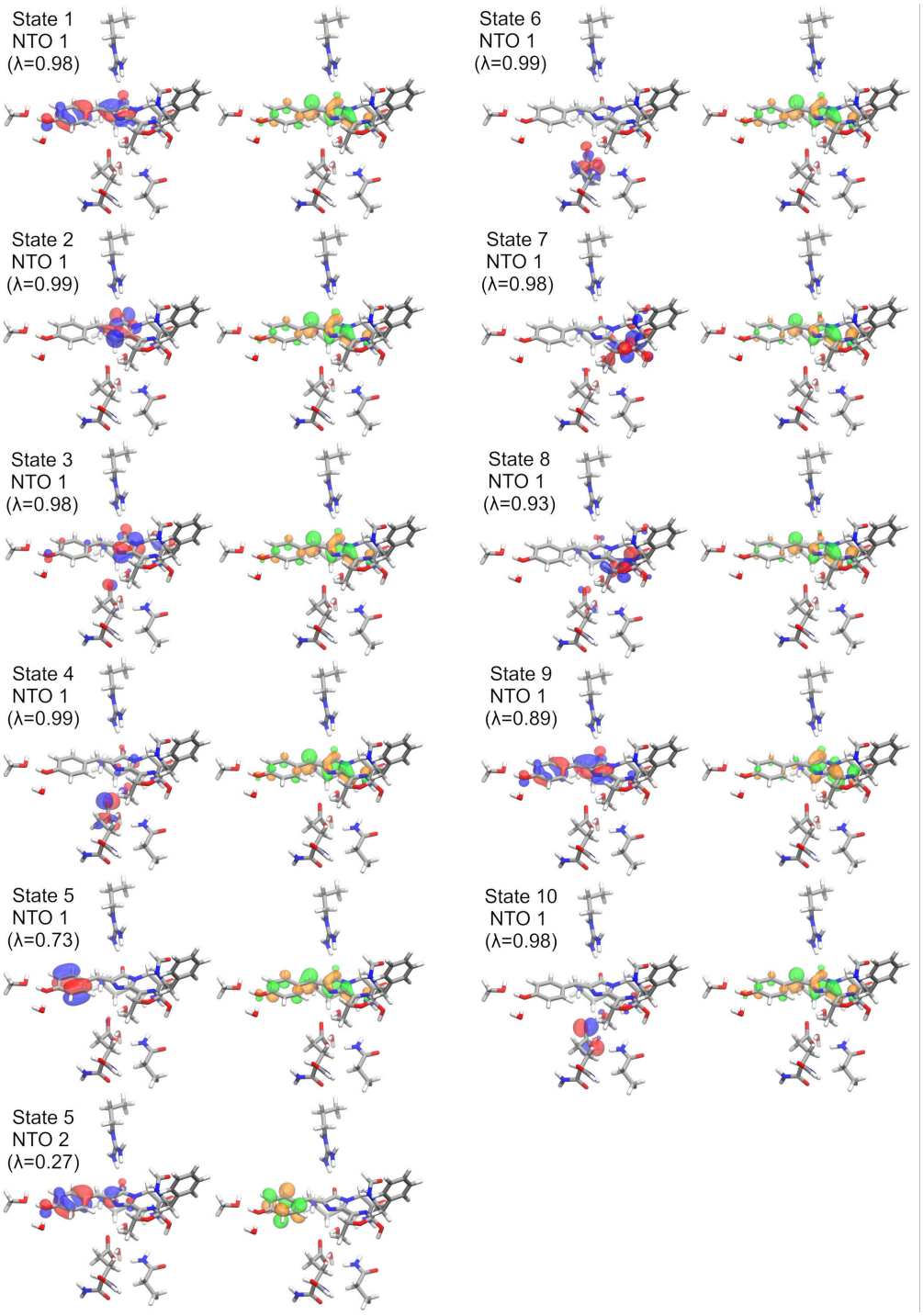

Figure S15: Most significant hole (red, blue) and electron (orange, green) NTOs of LSSmOrange excited states, calculated with RVS-CC2/def2-TZVP, corresponding to Figure S14.

EGFP

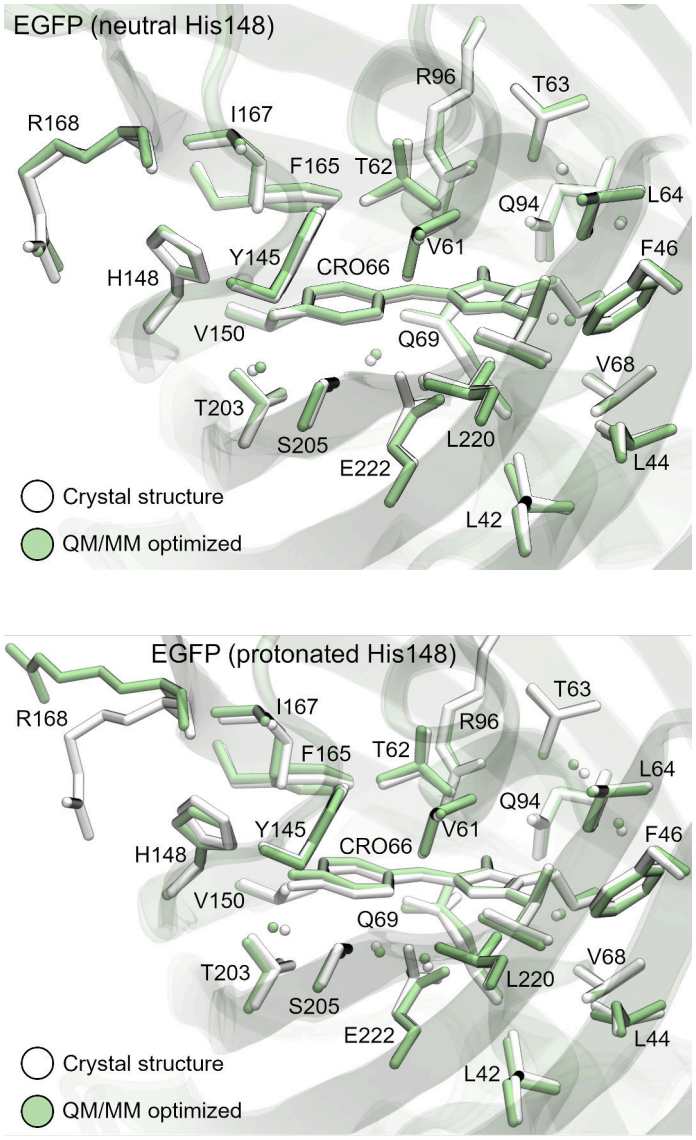

Figure S16: Comparison of QM/MM optimized (green; neutral His148 at top, protonated His148 at bottom) and crystal (white, PDB: 2Y0G[3]) structure of EGFP. The chromophore and nearby amino acids are shown as sticks and nearby water molecules as spheres. Hydrogen atoms are omitted for clarity.

State	$\Delta E(S_0 \rightarrow S_n)$/eV	f
1	2.975	1.329
2	4.086	0.002
3	4.288	0.011
4	4.349	0.033
5	4.358	0.004
6	5.018	0.015
7	5.035	0.120
8	5.183	0.002
9	5.399	0.210
10	5.490	0.090

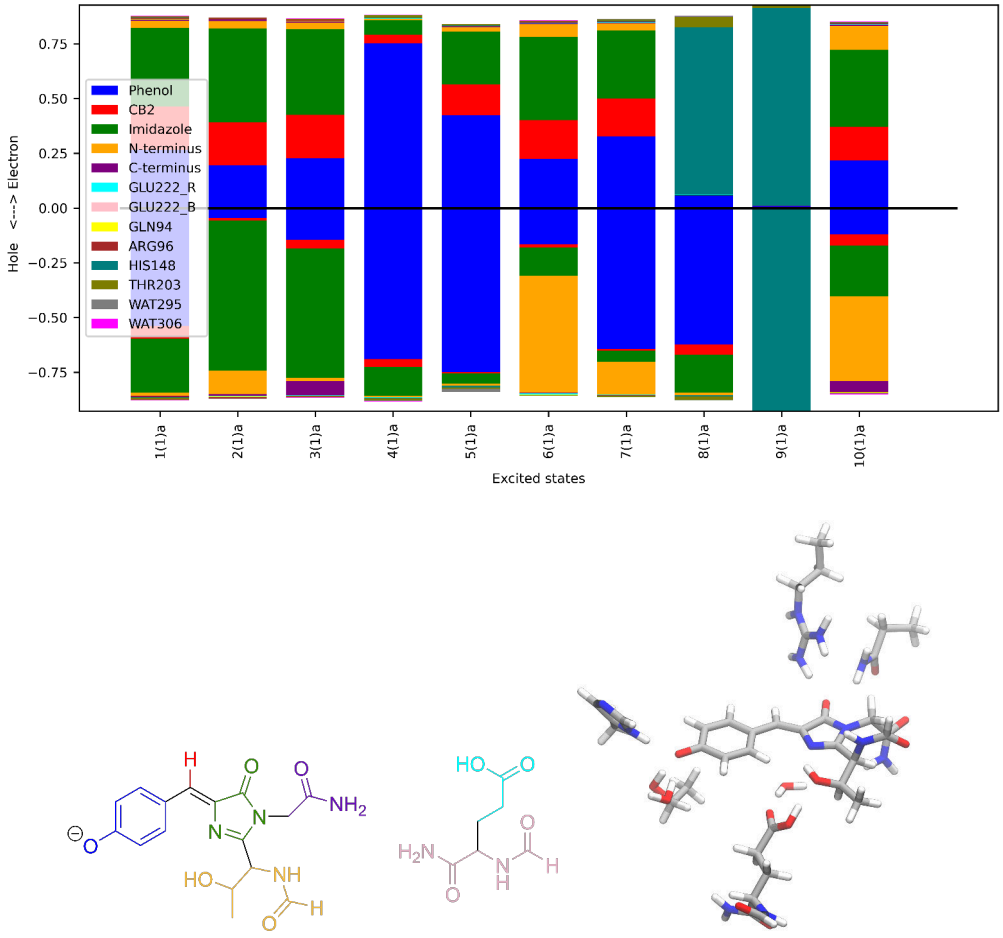

Figure S17: Fragment decomposition performed with TheoDORE of electron and hole populations of excited states of EGFP with neutral His148 calculated with CC2/def2-TZVP. Vertical excitation energies and oscillator strengths of each state are shown on the top. The QM region used in excited-state calculations and fragments corresponding to the chromophore and Glu222 are shown below, with colors matching those used in the plot.

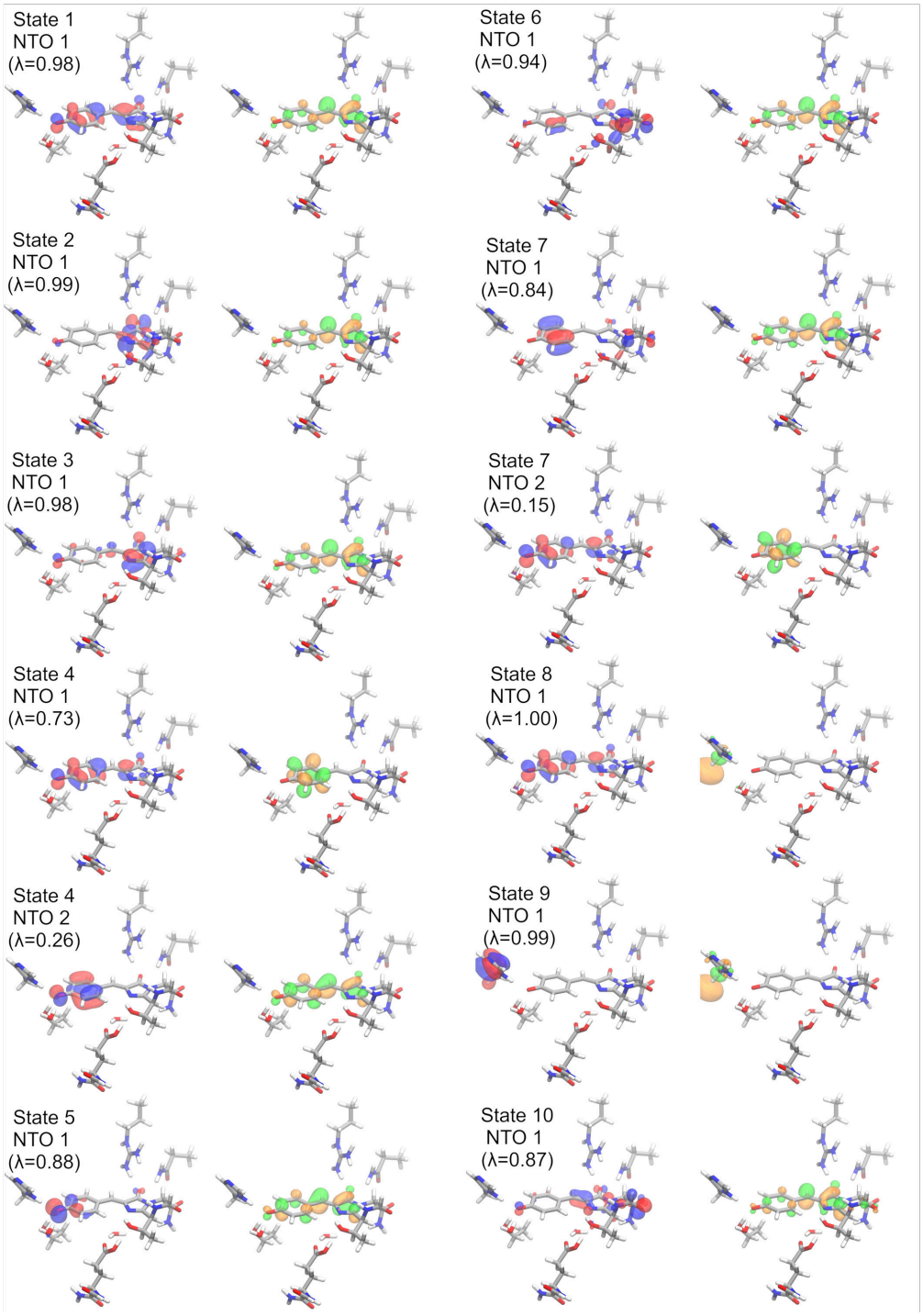

Figure S18: Most significant hole (red, blue) and electron (orange, green) NTOs of EGFP (neutral His148) excited states, calculated with RVS-CC2/def2-TZVP, corresponding to Figure S17.

State	$\Delta E(S_0 \rightarrow S_n)$/eV	f
1	3.218	1.263
2	4.454	0.003
3	4.562	0.019
4	4.681	0.017
5	5.044	0.242
6	5.118	0.002
7	5.175	0.102
8	5.223	0.002
9	5.297	0.042
10	5.680	0.022
11	5.786	0.043
12	5.799	0.012
13	5.870	0.000
14	5.921	0.004
15	5.945	0.003
16	5.957	0.003
17	6.064	0.018
18	6.080	0.003
19	6.104	0.003
20	6.171	0.035

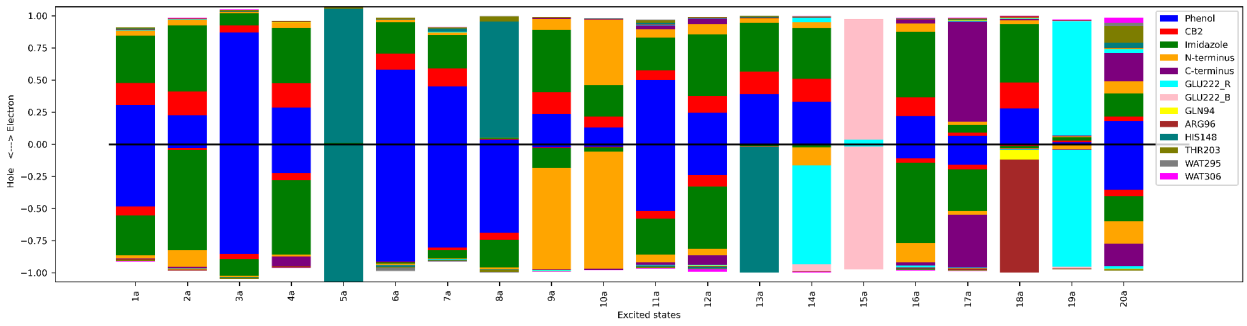

Figure S19: Fragment decomposition performed with TheoDORE of electron and hole populations of excited states of EGFP with neutral His148 calculated with CAM-B3LYP/def2-TZVP. Vertical excitation energies and oscillator strengths of each state are shown on the top. The QM region used in excited-state calculations and fragments corresponding to the chromophore and Glu222 are shown in Figure S17.

State	$\Delta E(S_0 \rightarrow S_n)$/eV	f
1	2.893	1.312
2	4.189	0.003
3	4.374	0.019
4	4.394	0.008
5	4.420	0.001
6	4.913	0.076
7	5.135	0.083
8	5.452	0.050
9	5.542	0.055
10	5.583	0.095

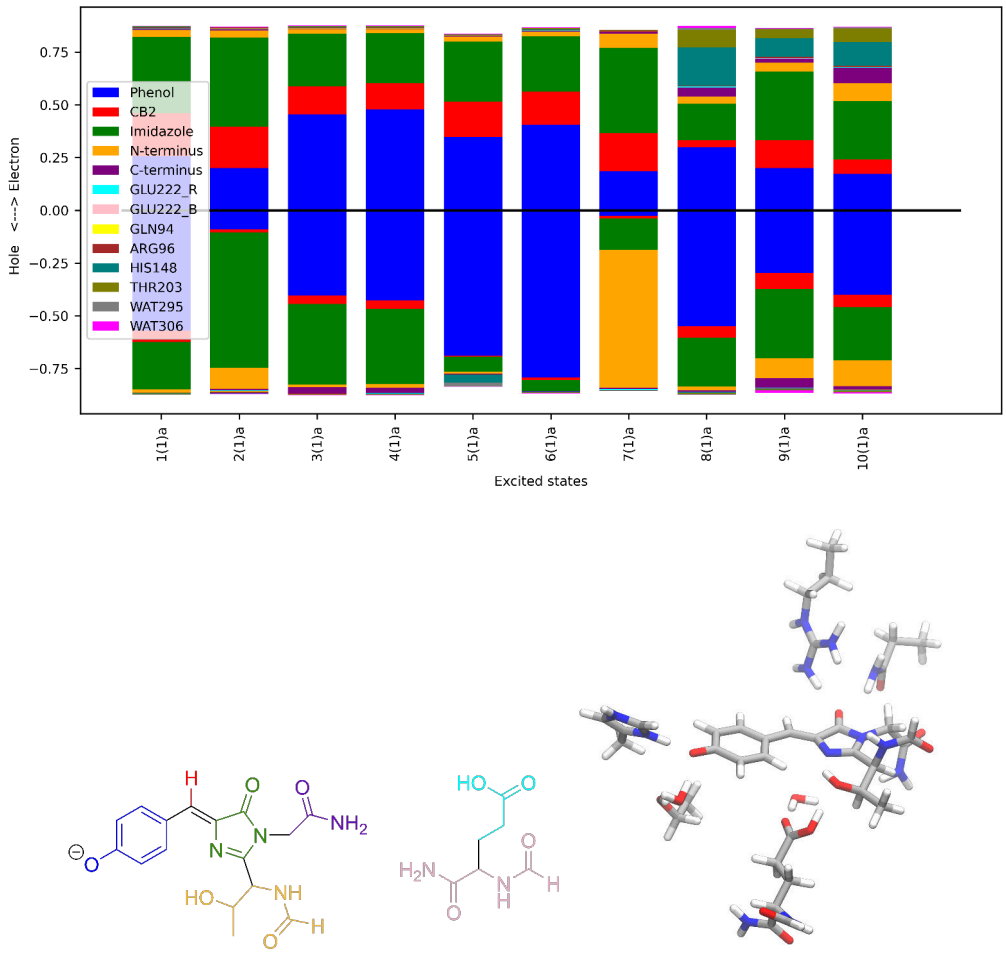

Figure S20: Fragment decomposition performed with TheoDORE of electron and hole populations of excited states of EGFP with protonated His148 calculated with CC2/def2-TZVP. Vertical excitation energies and oscillator strengths of each state are shown on the top. The QM region used in excited-state calculations and fragments corresponding to the chromophore and Glu222 are shown below, with colors matching those used in the plot.

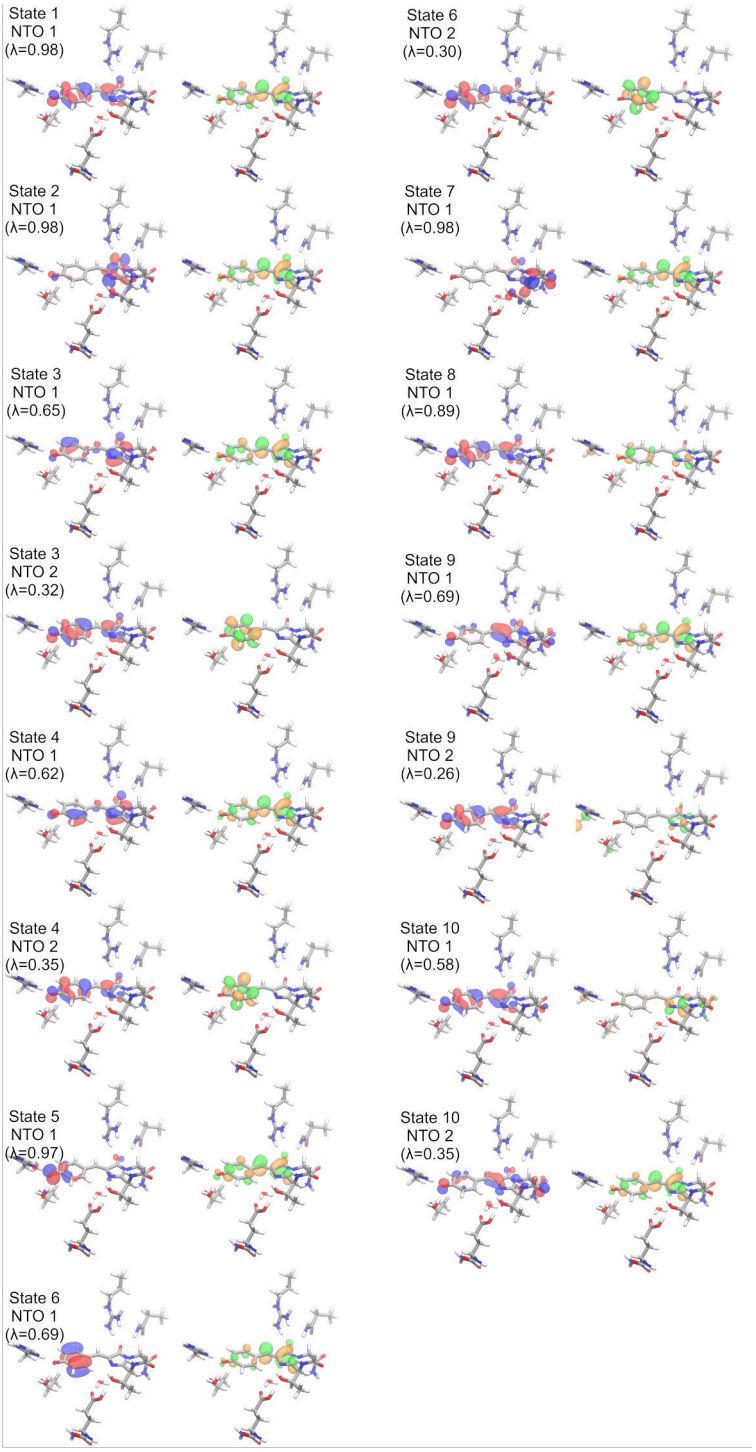

Figure S21: Most significant hole (red, blue) and electron (orange, green) NTOs of EGFP (protonated His148) excited states, calculated with RVS-CC2/def2-TZVP, corresponding to Figure S20.

State	$\Delta E(S_0 \rightarrow S_n)$/eV	f
1	3.183	1.253
2	4.542	0.003
3	4.573	0.007
4	4.752	0.007
5	5.103	0.114
6	5.214	0.001
7	5.419	0.049
8	5.629	0.012
9	5.677	0.022
10	5.748	0.027
11	5.750	0.120
12	5.798	0.014
13	5.818	0.008
14	5.869	0.003
15	5.903	0.021
16	5.948	0.000
17	5.966	0.001
18	5.977	0.005
19	6.017	0.004
20	6.041	0.007

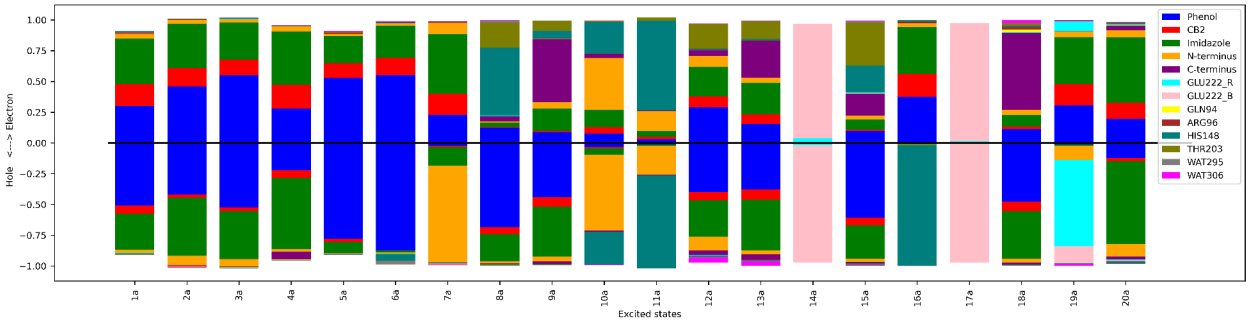

Figure S22: Fragment decomposition performed with TheoDORE of electron and hole populations of excited states of EGFP with protonated His148 calculated with CAM-B3LYP/def2-TZVP. Vertical excitation energies and oscillator strengths of each state are shown on the top. The QM region used in excited-state calculations and fragments corresponding to the chromophore and Glu222 are shown in Figure S20.

DsRed

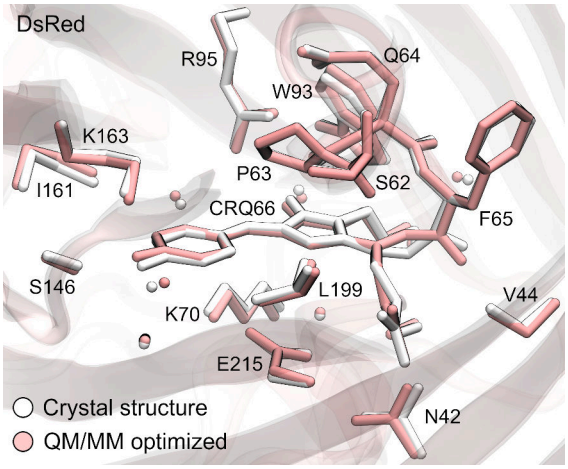

Figure S23: Comparison of QM/MM optimized (pink) and crystal (white, PDB: 1ZGO[4]) structure of DsRed. The chromophore and nearby amino acid residues are shown as sticks and nearby water molecules as spheres. Hydrogen atoms are omitted for clarity.

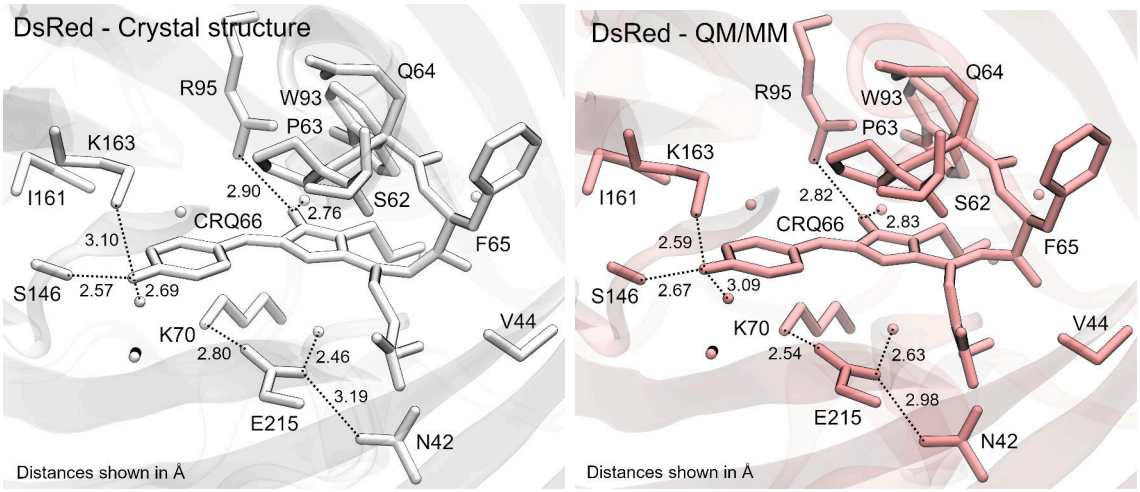

Figure S24: Comparison of H-bond networks in QM/MM optimized (pink) and crystal (white, PDB: 1ZGO[4]) structure of DsRed. The chromophore and nearby amino acid residues are shown as sticks and nearby water molecules as spheres. Hydrogen atoms are omitted for clarity.

State	$\Delta E(S_0 \rightarrow S_n)$/eV	f
1	2.657	1.314
2	3.879	0.002
3	4.016	0.003
4	4.119	0.011
5	4.165	0.009
6	4.331	0.036
7	4.350	0.171
8	4.781	0.082
9	4.906	0.036
10	5.010	0.000

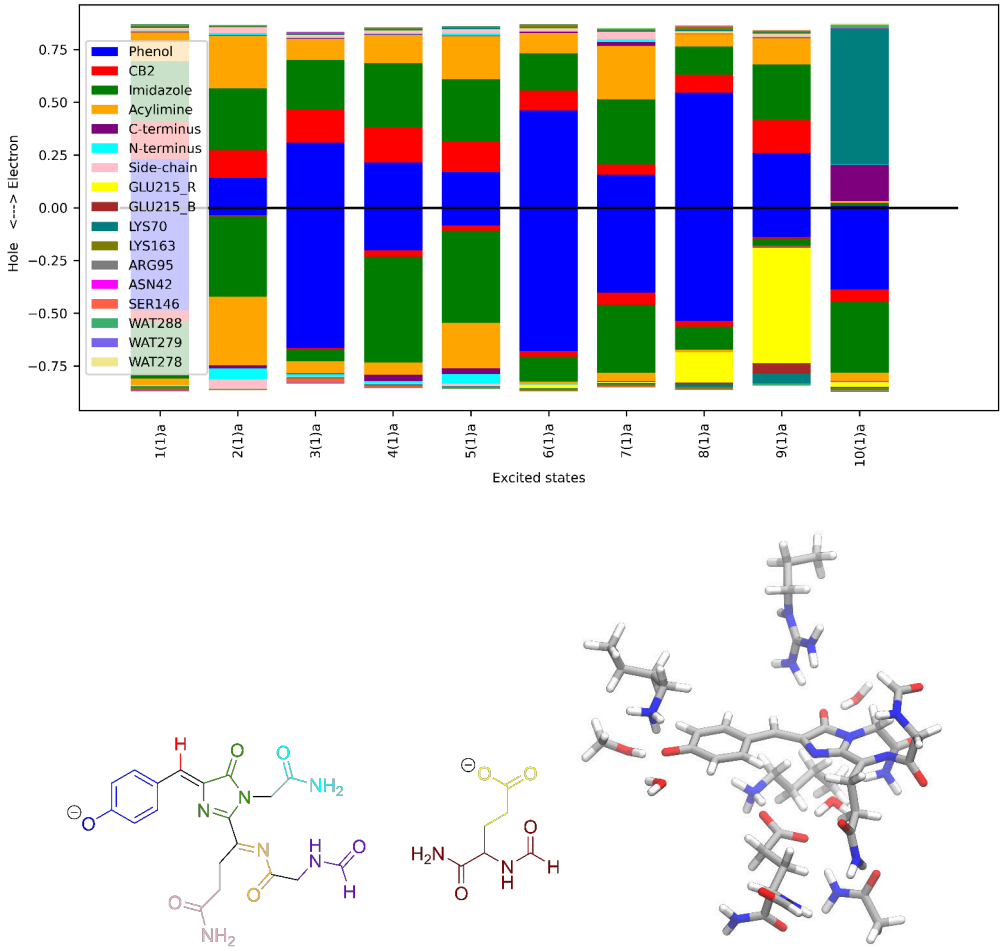

Figure S25: Fragment decomposition performed with TheoDORE of electron and hole populations of excited states of DsRed calculated with CC2/def2-TZVP. Vertical excitation energies and oscillator strengths of each state are shown on the top. The QM region used in the excited-state calculations and fragments corresponding to the chromophore and Glu215 are shown below, with colors matching those used in the plot.

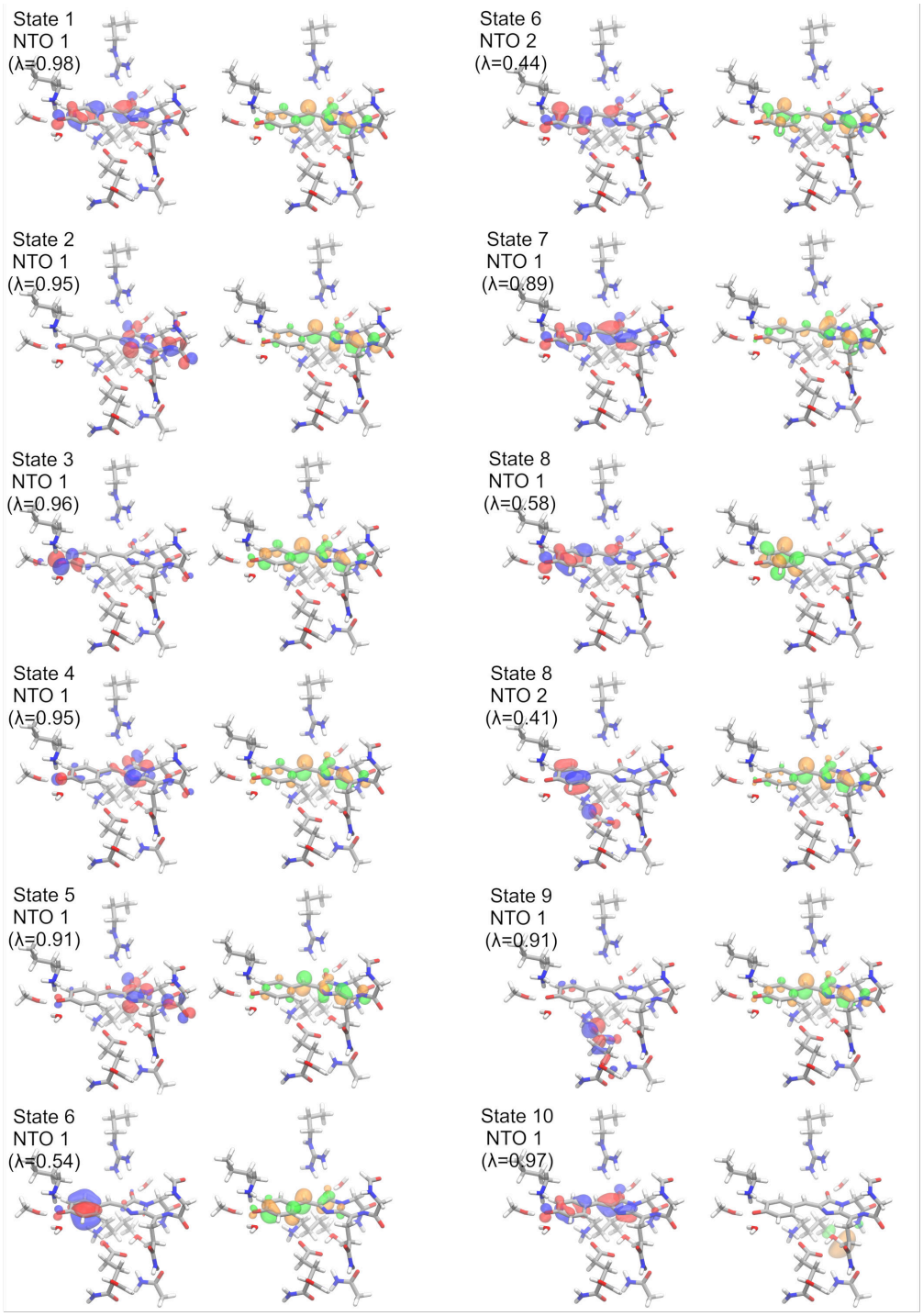

Figure S26: Most significant hole (red, blue) and electron (orange, green) NTOs of DsRed excited states, calculated with RVS-CC2/def2-TZVP, corresponding to Figure S25.

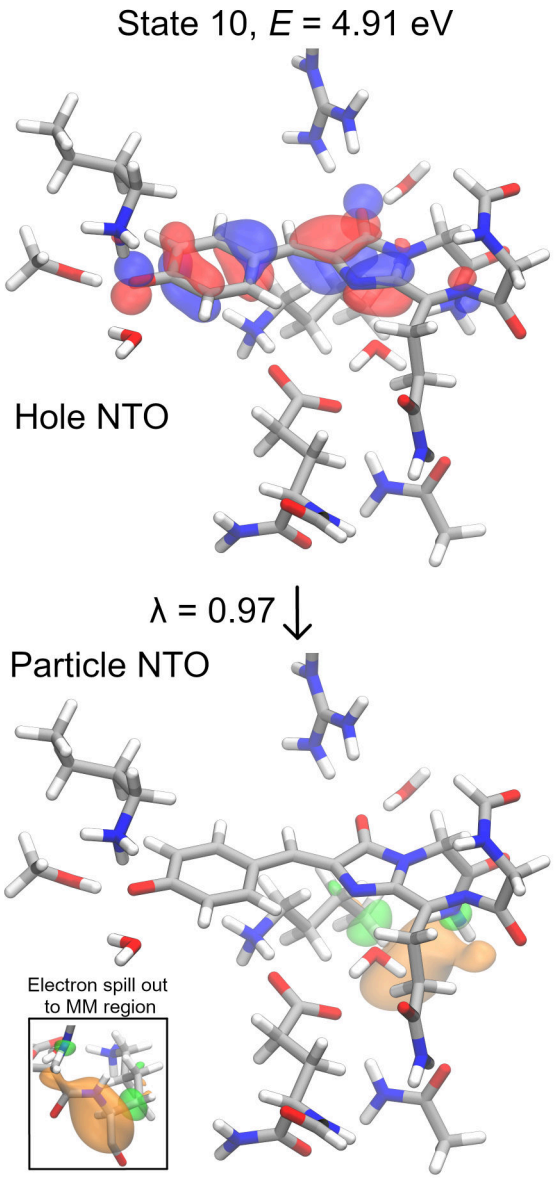

Figure S27: NTOs of the tenth excited state in DsRed calculated with CC2/def2-TZVP. The rest of the system, not shown here, was described with polarizable embedding. Insert shows that the electron density spilled out to the backbone of Lys70 which was not included in the QM region.

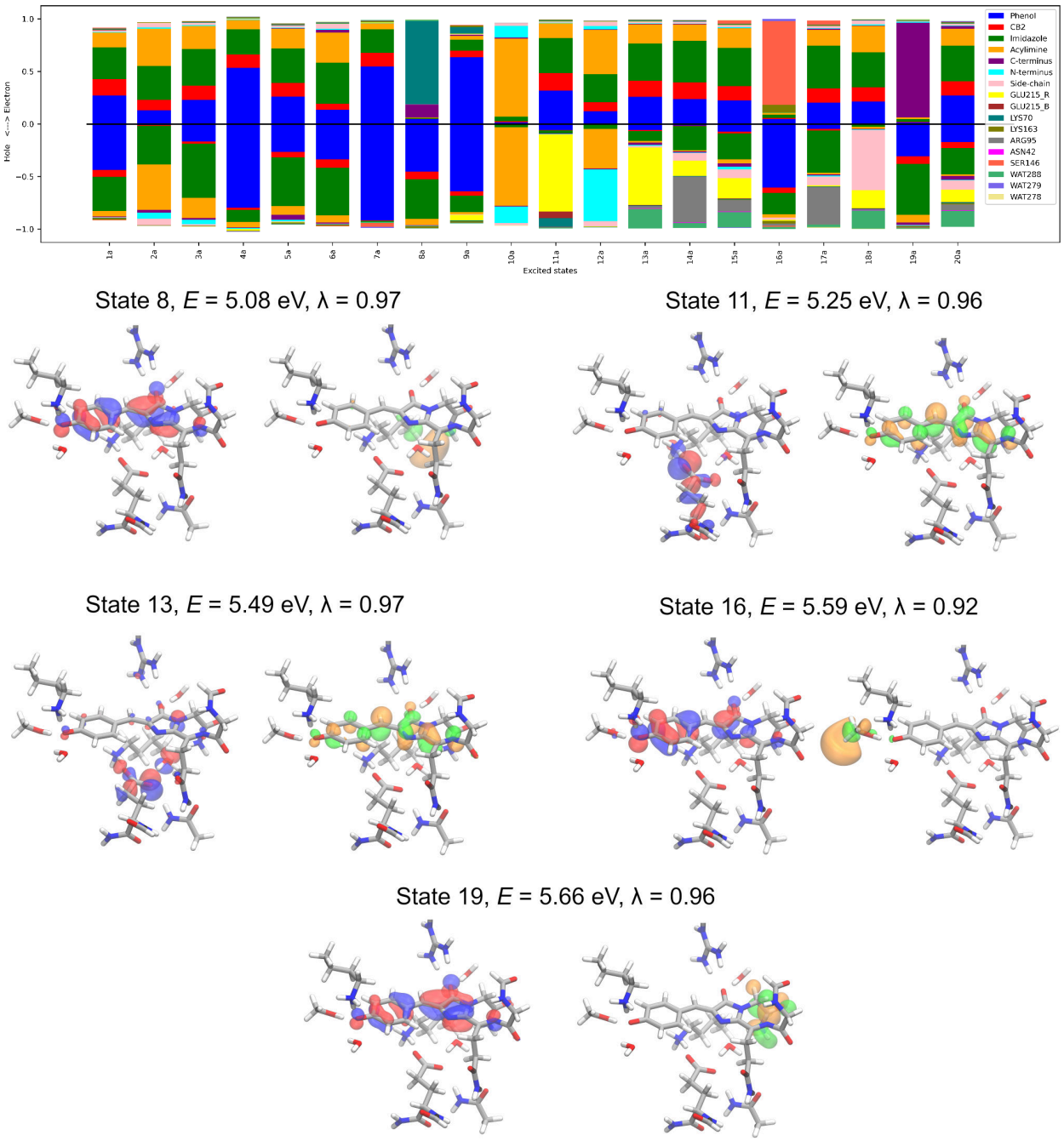

Figure S28: Fragment decomposition performed with TheoDORE of electron and hole populations of excited states of DsRed calculated with CAM-B3LYP/def2-TZVP (top) and dominant hole-particle NTO pairs of some selected states (bottom). Fragment definitions of the chromophore and Glu215 are shown in Figure S25.

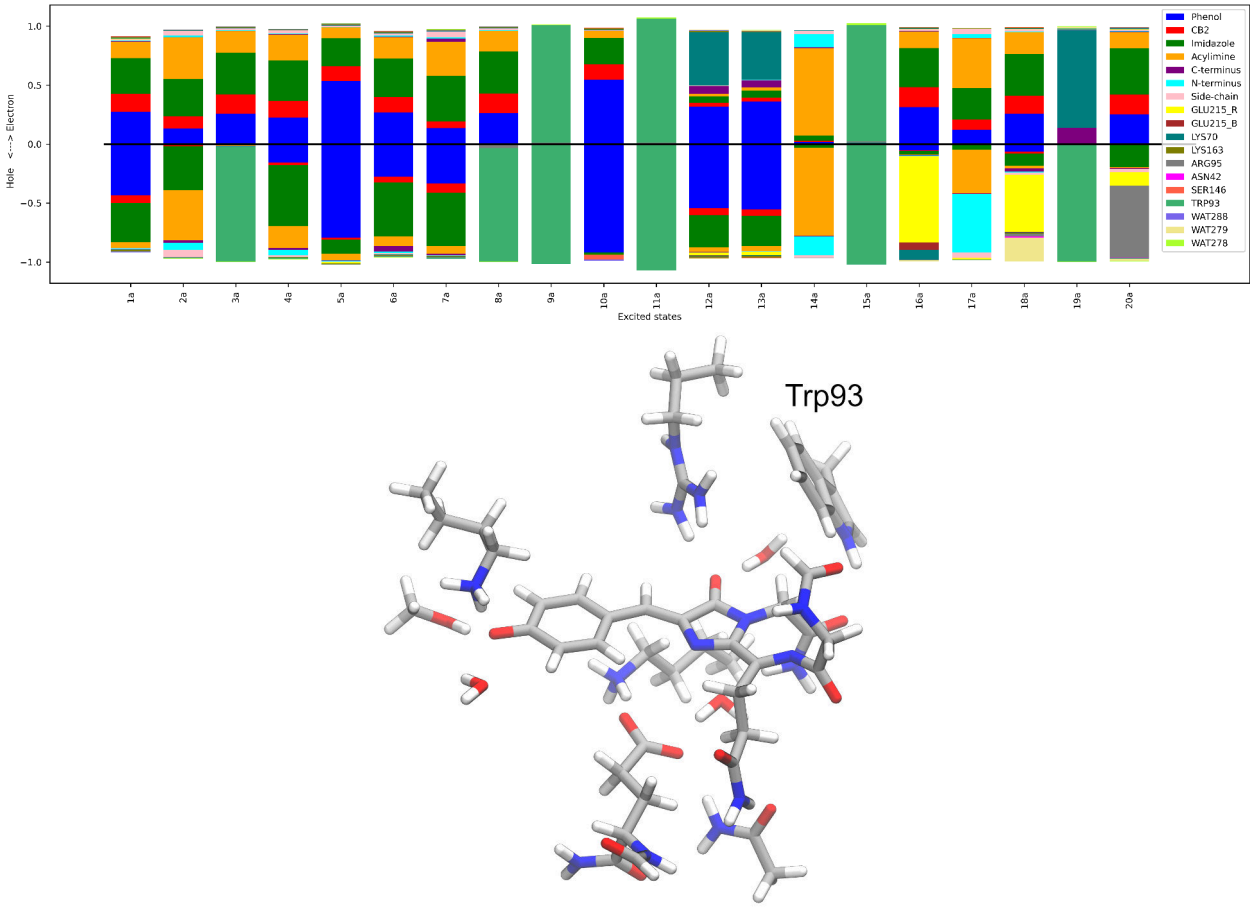

Figure S29: Fragment decomposition performed with TheoDORE of electron and hole populations of excited states of DsRed calculated with CAM-B3LYP/def2-TZVP (top) with an expanded QM region containing the side-chain of Trp93 (bottom). The rest of the system was treated with polarizable embedding. Fragment definitions of the chromophore and Glu215 are shown in Figure S25.

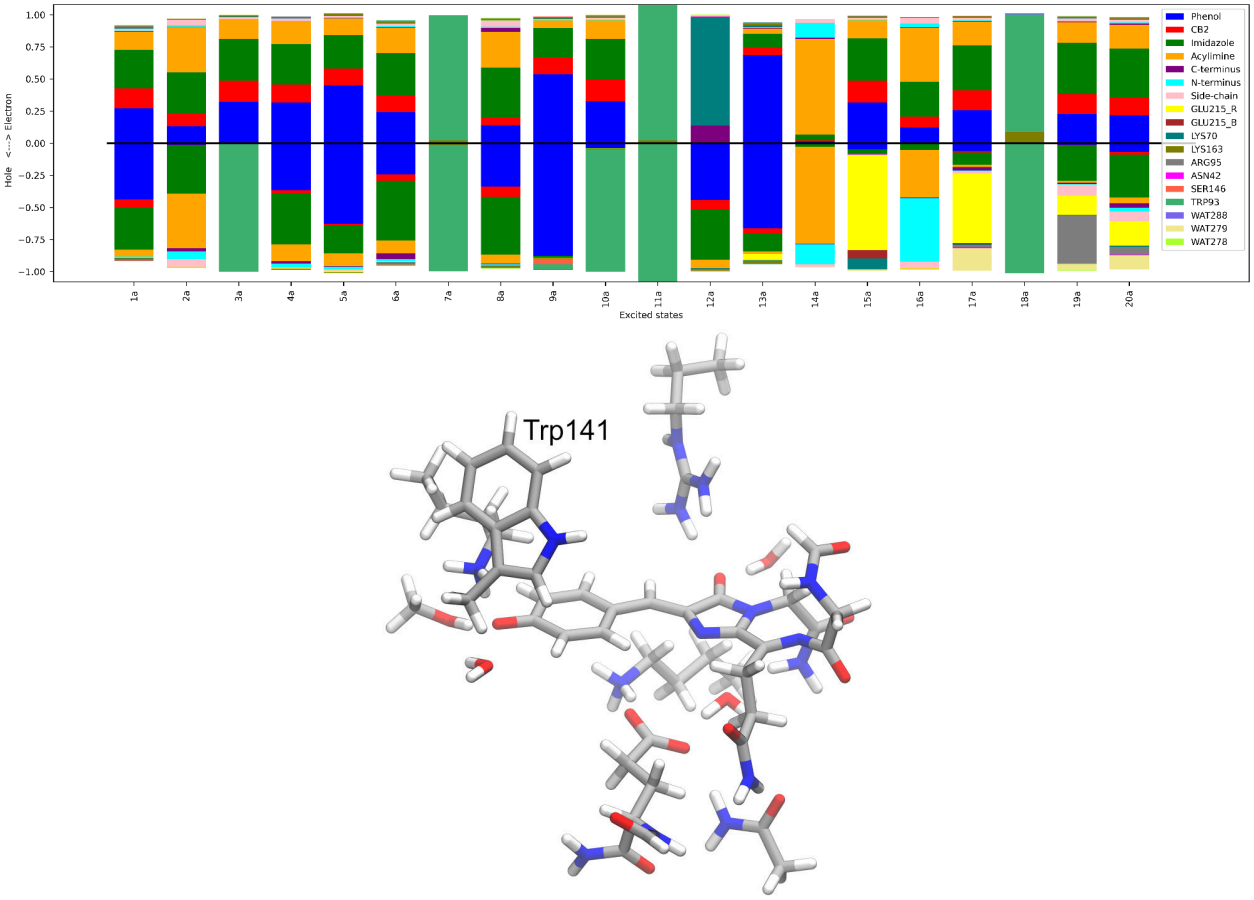

Figure S30: Fragment decomposition performed with TheoDORE of electron and hole populations of excited states of DsRed calculated with CAM-B3LYP/def2-TZVP (top) with an expanded QM region containing the side-chain of Trp141 (bottom). The rest of the system was treated with polarizable embedding. Fragment definitions of the chromophore and Glu215 are shown in Figure S25.

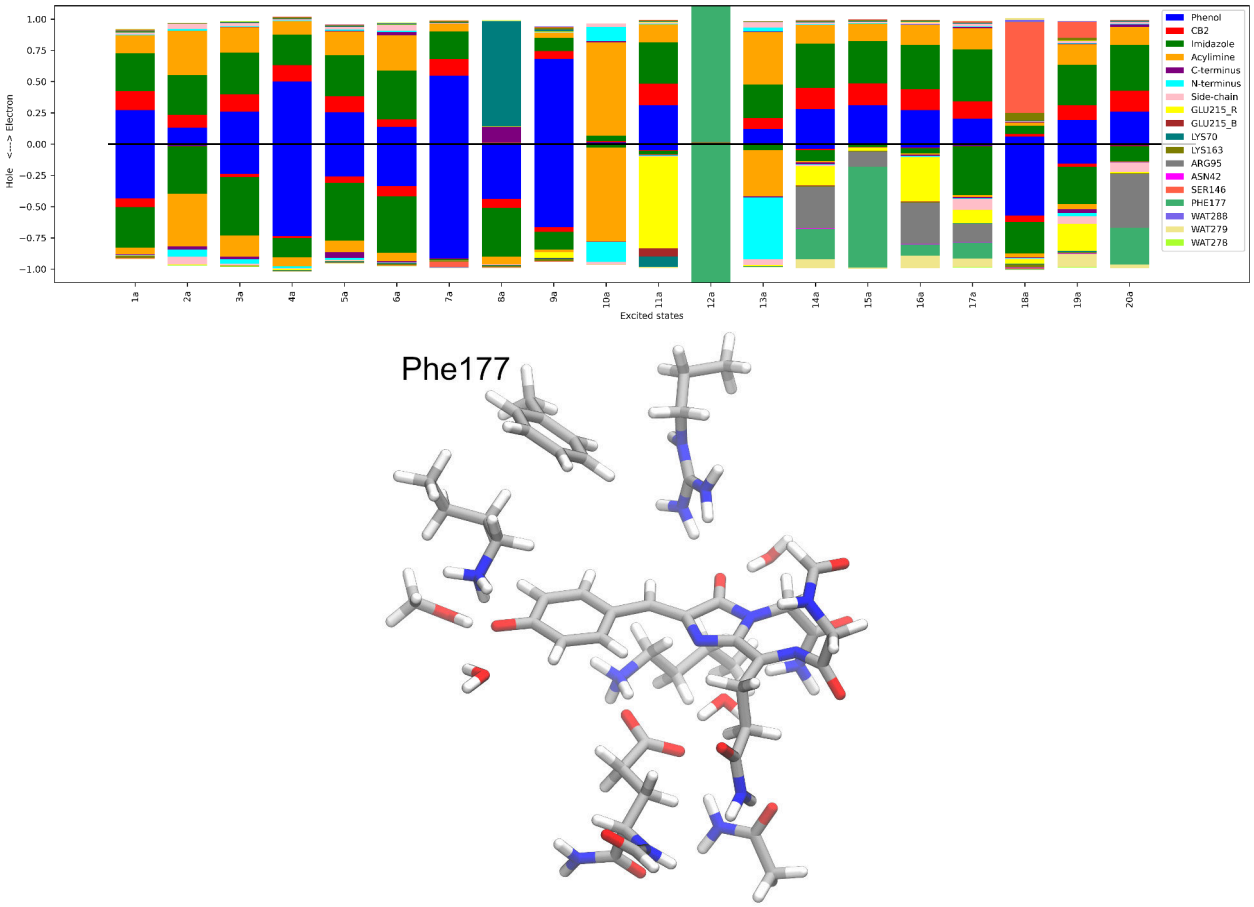

Figure S31: Fragment decomposition performed with TheoDORE of electron and hole populations of excited states of DsRed calculated with CAM-B3LYP/def2-TZVP (top) with an expanded QM region containing the side-chain of Phe177 (bottom). The rest of the system was treated with polarizable embedding. Fragment definitions of the chromophore and Glu215 are shown in Figure S25.

LSSmKate1

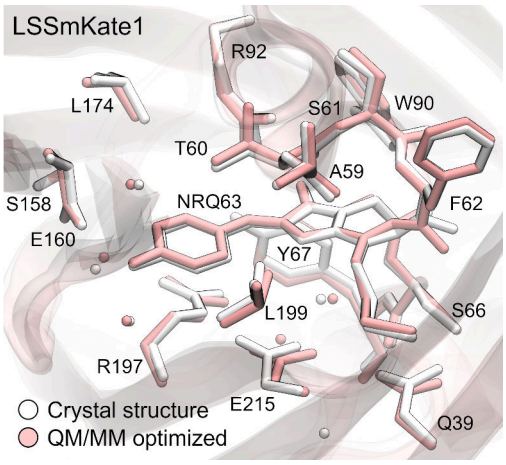

Figure S32: Comparison of QM/MM optimized (pink) and crystal (white, PDB: 3NT9[5]) structure of LSSmKate1. The chromophore and nearby amino acid residues are shown as sticks and nearby water molecules as spheres. Hydrogen atoms are omitted for clarity.

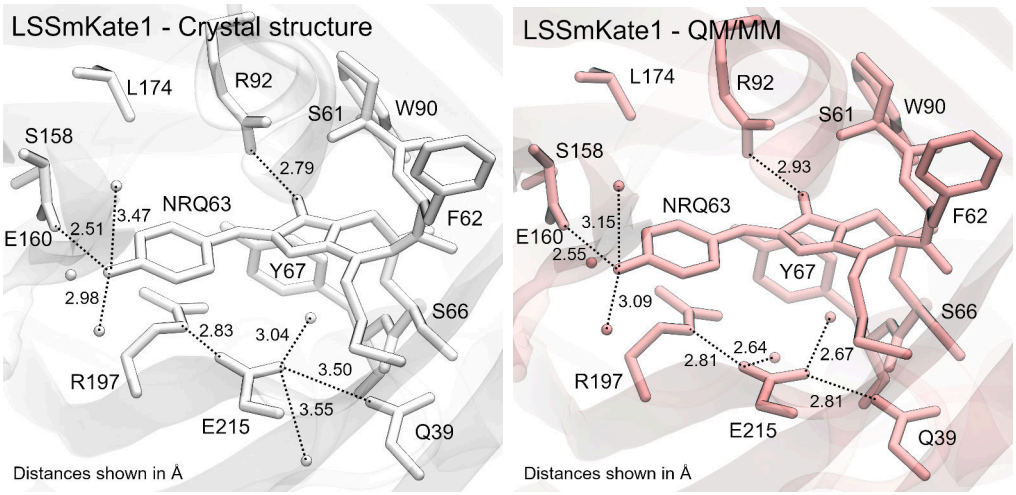

Figure S33: Comparison of H-bond networks in QM/MM optimized (pink) and crystal (white, PDB: 3NT9[5]) structure of LSSmKate1. The chromophore and nearby amino acid residues are shown as sticks and nearby water molecules as spheres. Hydrogen atoms are omitted for clarity.

State	$\Delta E(S_0 \rightarrow S_n)$/eV	f
1	3.017	0.978
2	3.697	0.003
3	3.914	0.002
4	4.124	0.037
5	4.421	0.001
6	4.651	0.193
7	4.715	0.008
8	4.826	0.005
9	4.857	0.001
10	5.066	0.149

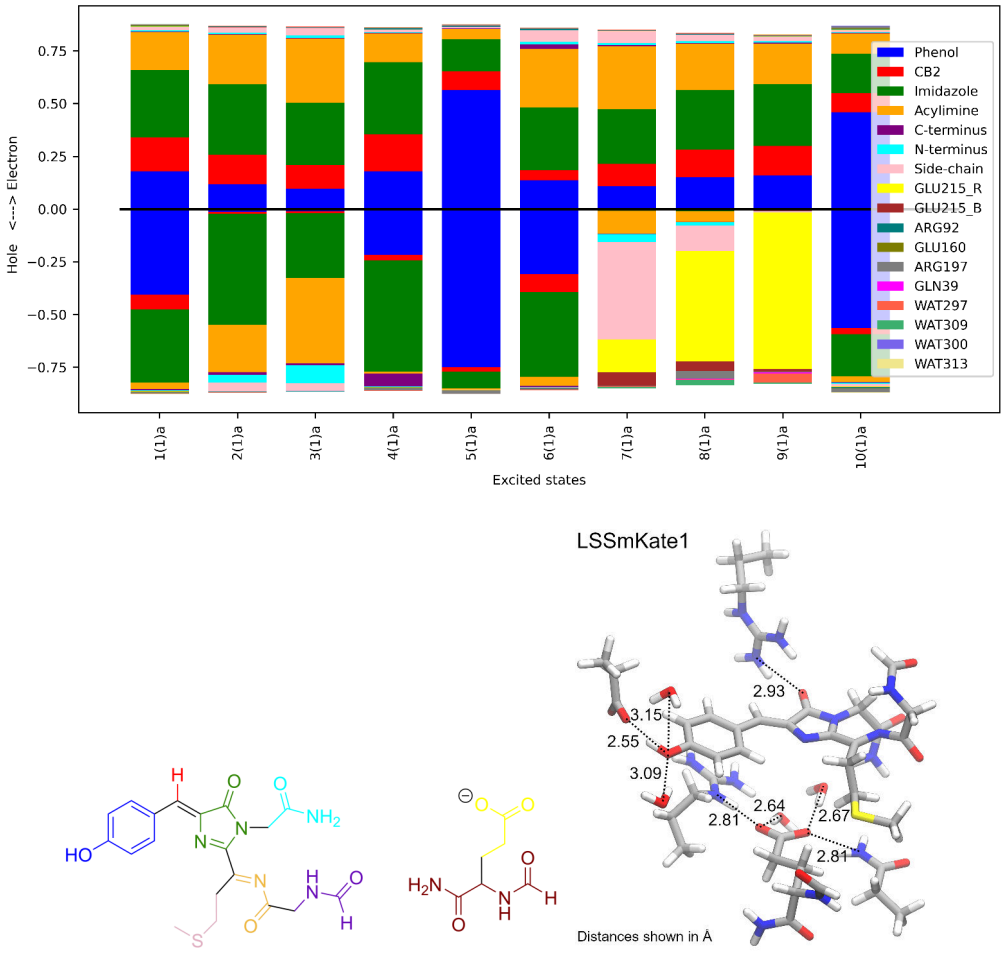

Figure S34: Fragment decomposition performed with TheoDORE of electron and hole populations of excited states of LSSmKate1 calculated with CC2/def2-TZVP. Vertical excitation energies and oscillator strengths of each state are shown on the top. The QM region used in excited-state calculations and fragments corresponding to the chromophore and Glu215 are shown below, with colors matching those used in the plot.

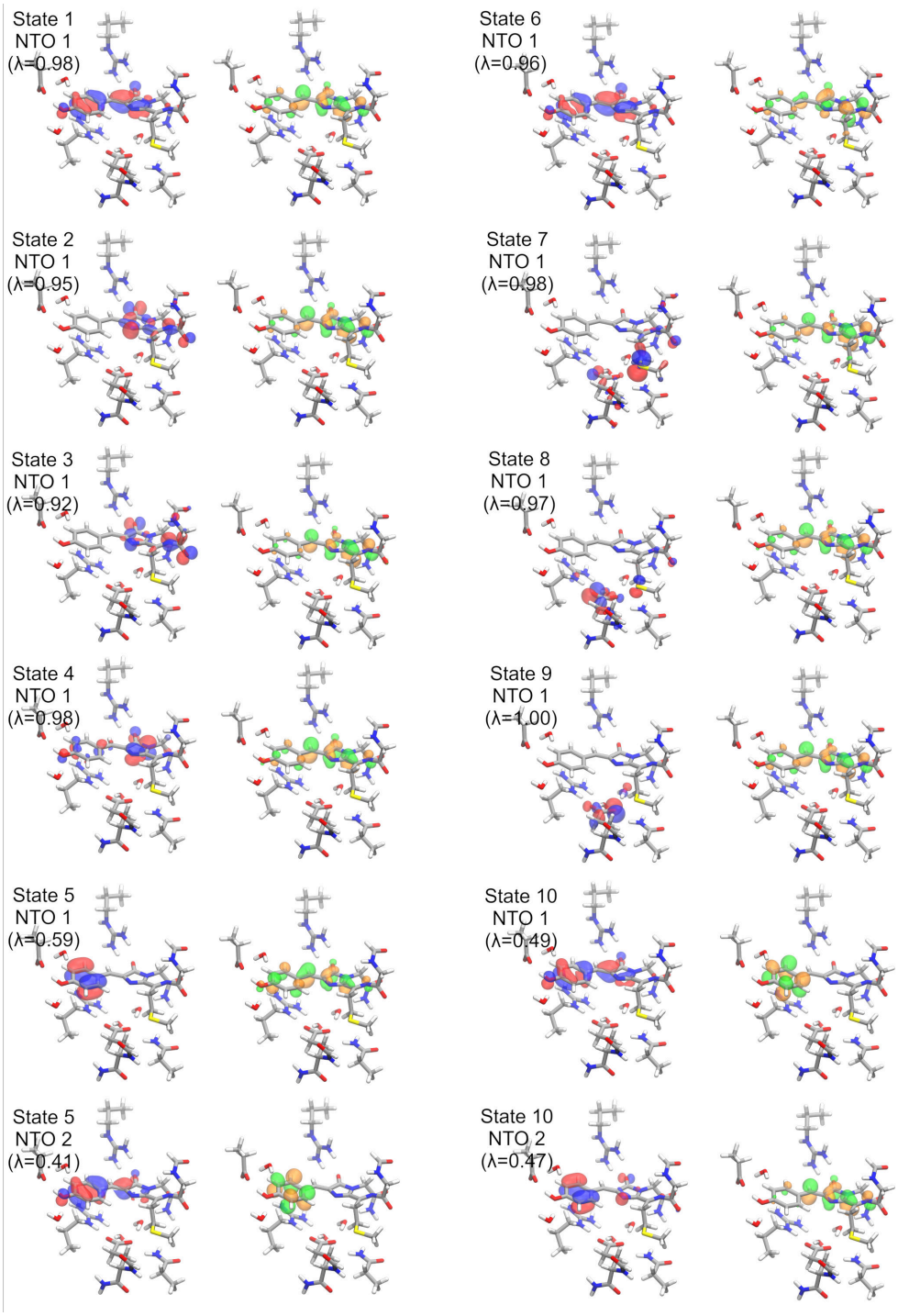

Figure S35: Most significant hole (red, blue) and electron (orange, green) NTOs of LSSmKate1 excited states, calculated with RVS-CC2/def2-TZVP, corresponding to Figure S34.

State	$\Delta E(S_0 \rightarrow S_n)$/eV	f
1	3.151	0.960
2	3.987	0.002
3	4.240	0.002
4	4.493	0.035
5	4.599	0.001
6	4.729	0.005
7	4.882	0.133
8	5.079	0.008
9	5.242	0.024
10	5.258	0.078
11	5.293	0.068
12	5.362	0.001
13	5.378	0.005
14	5.423	0.003
15	5.448	0.012
16	5.645	0.011
17	5.670	0.006
18	5.708	0.059
19	5.750	0.004
20	5.752	0.007
21	5.779	0.027
22	5.807	0.029
23	5.840	0.002
24	5.873	0.011
25	5.900	0.006

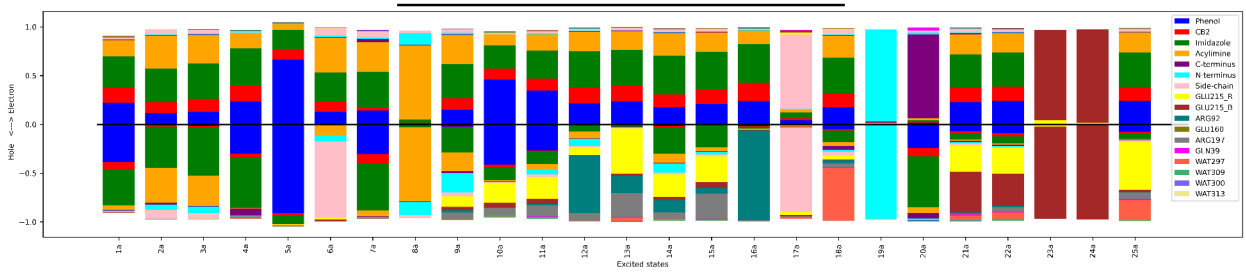

Figure S36: Fragment decomposition performed with TheoDORE of electron and hole populations of excited states of LSSmKate1 calculated with CAM-B3LYP/def2-TZVP. Vertical excitation energies and oscillator strengths of each state are shown on the top. The QM region used in excited-state calculations and fragments corresponding to the chromophore and Glu215 are shown in Figure S34.

PSLSSmKate

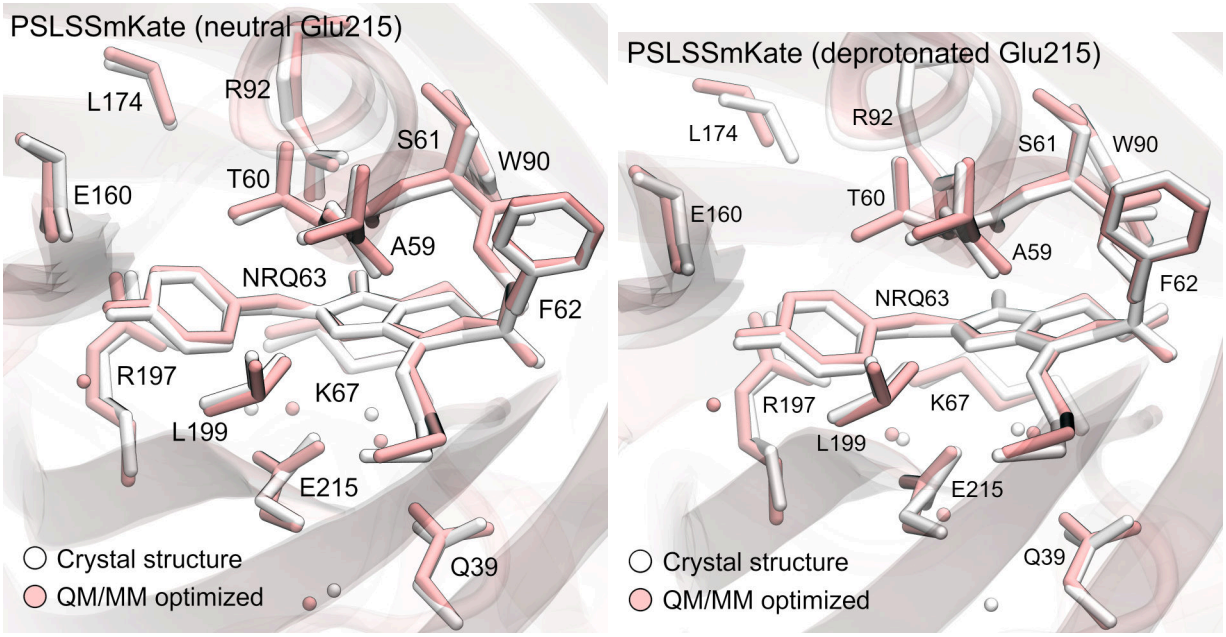

Figure S37: Comparison of QM/MM optimized (pink) and crystal (white, PDB: 4NWS[6]) structure of PSLSSmKate if Glu215 is considered neutral (left) or deprotonated (right). The chromophore and nearby amino acid residues are shown as sticks and nearby water molecules as spheres. Hydrogen atoms are omitted for clarity.

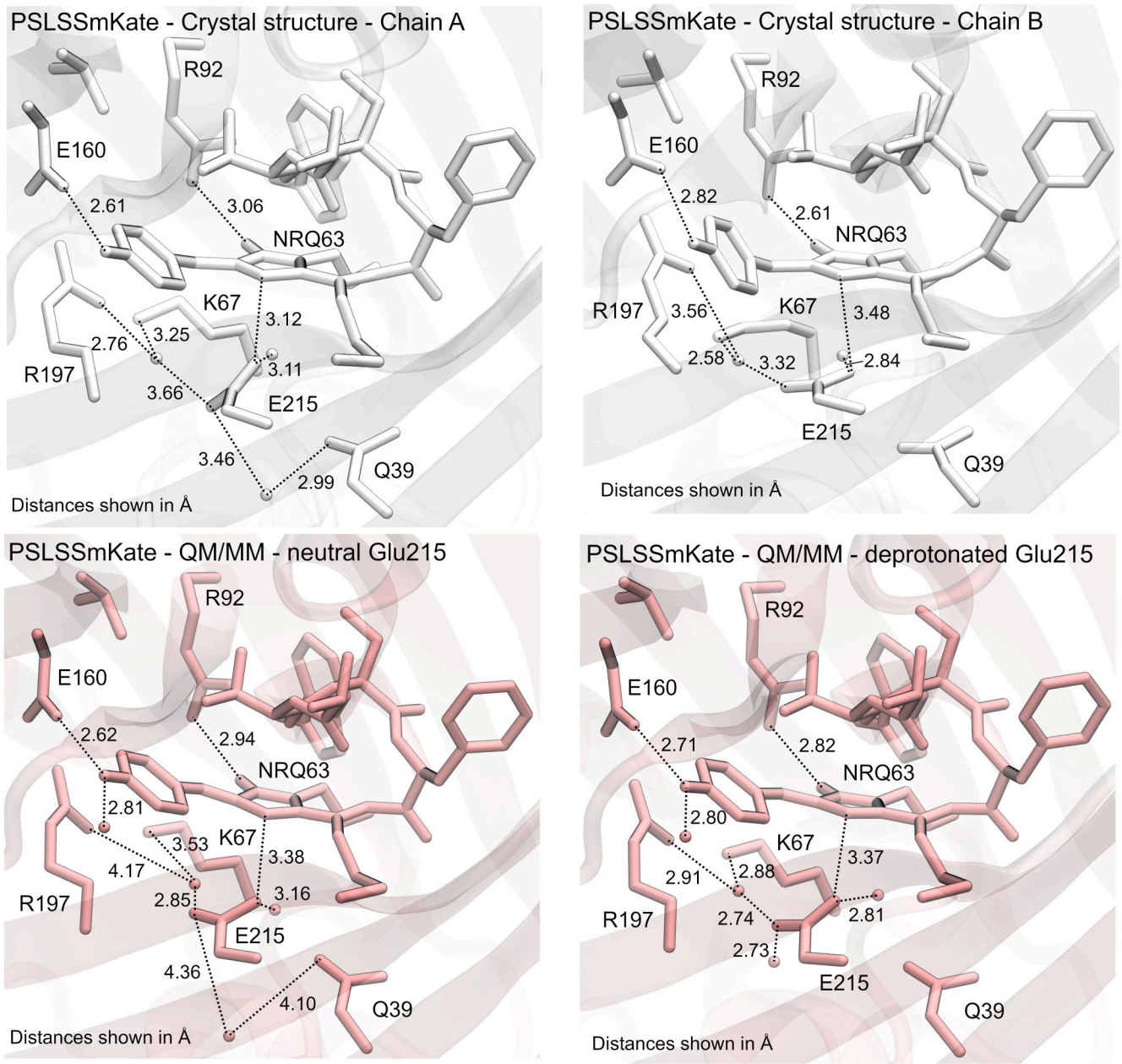

Figure S38: Comparison of H-bond networks in QM/MM optimized (pink) and crystal (white, chains A and B, PDB: 4NWS[6]) structure of PSLSSmKate if Glu215 is considered neutral or deprotonated. The chromophore and nearby amino acid residues are shown as sticks and nearby water molecules as spheres. Hydrogen atoms are omitted for clarity.

State	$\Delta E(S_0 \rightarrow S_n)$/eV	f
1	2.850	1.058
2	3.729	0.002
3	3.937	0.002
4	4.151	0.010
5	4.328	0.002
6	4.544	0.039
7	4.550	0.181
8	4.970	0.043
9	4.997	0.105
10	5.168	0.034

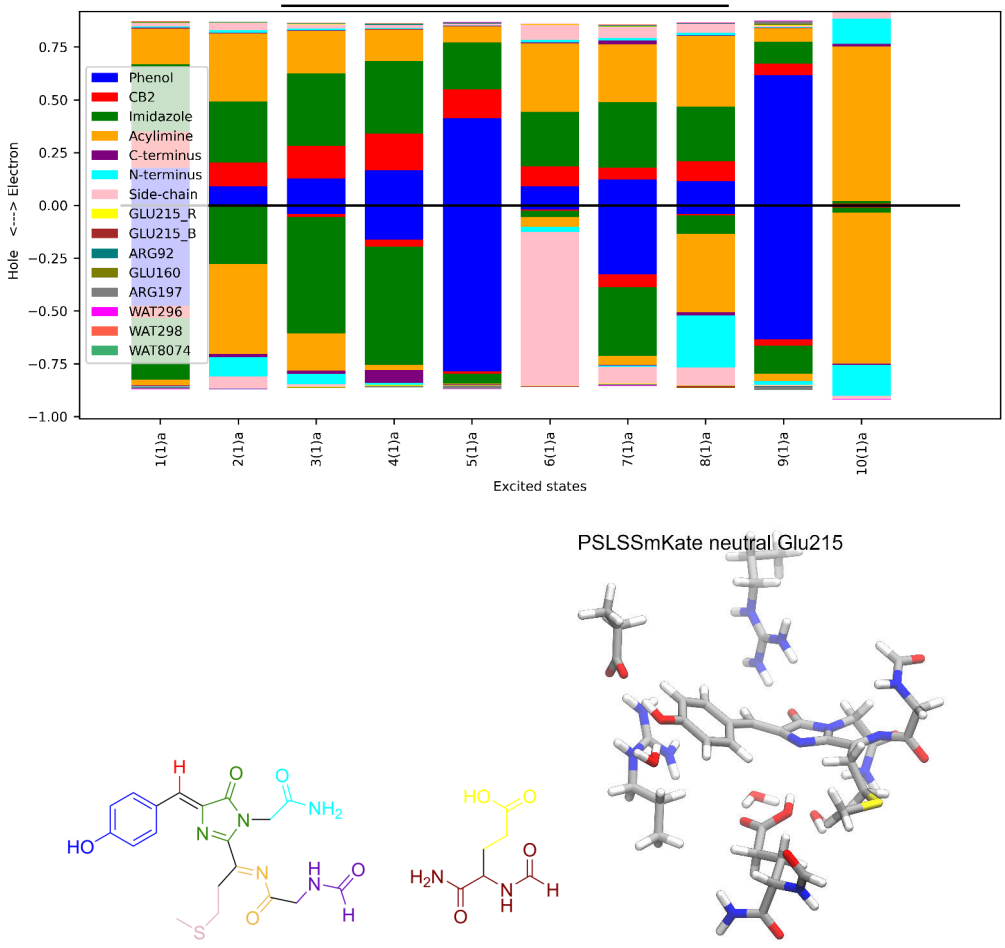

Figure S39: Fragment decomposition performed with TheoDORE of electron and hole populations of excited states of PSLSSmKate with neutral Glu215 calculated with CC2/def2-TZVP. Vertical excitation energies and oscillator strengths of each state are shown on the top. The QM region used in excited-state calculations and fragments corresponding to the chromophore and Glu215 are shown below, with colors matching those used in the plot.

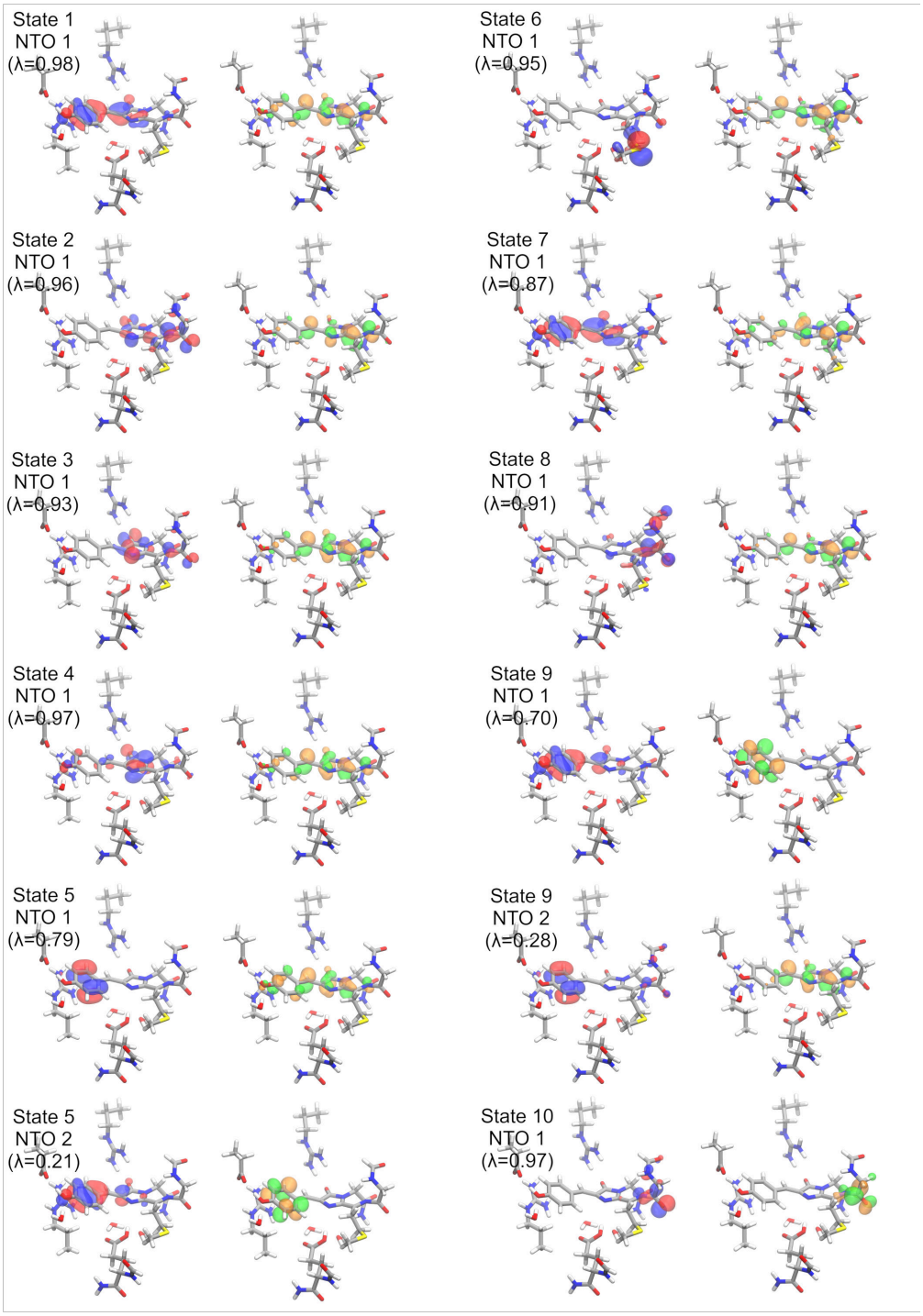

Figure S40: Most significant hole (red, blue) and electron (orange, green) NTOs of PSLSSmKate (neutral Glu215) excited states, calculated with RVS-CC2/def2-TZVP, corresponding to Figure S39.

State	$\Delta E(S_0 \rightarrow S_n)$/eV	f
1	3.067	1.038
2	3.998	0.001
3	4.290	0.005
4	4.411	0.004
5	4.485	0.004
6	4.531	0.021
7	4.822	0.141
8	5.073	0.003
9	5.125	0.015
10	5.229	0.133
11	5.322	0.000
12	5.384	0.005
13	5.461	0.053
14	5.496	0.014
15	5.524	0.003
16	5.589	0.001
17	5.597	0.004
18	5.606	0.000
19	5.638	0.003
20	5.638	0.002
21	5.704	0.007
22	5.824	0.020
23	5.866	0.064
24	5.922	0.002
25	5.957	0.004

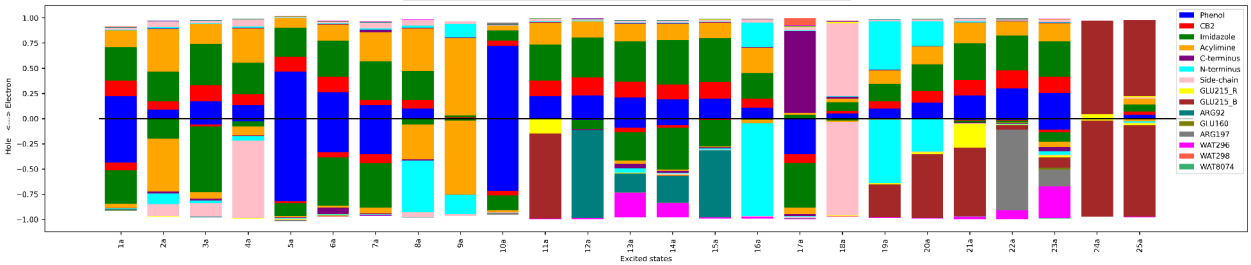

Figure S41: Fragment decomposition performed with TheoDORE of electron and hole populations of excited states of PSLSSmKate with neutral Glu215 calculated with CAM-B3LYP/def2-TZVP. Vertical excitation energies and oscillator strengths of each state are shown on the top. The QM region used in excited-state calculations and fragments corresponding to the chromophore and Glu215 are shown in Figure S39.

State	$\Delta E(S_0 \rightarrow S_n)$/eV	f
1	3.120	0.954
2	3.663	0.018
3	3.798	0.002
4	4.003	0.004
5	4.089	0.003
6	4.194	0.016
7	4.435	0.000
8	4.547	0.004
9	4.572	0.005
10	4.798	0.145

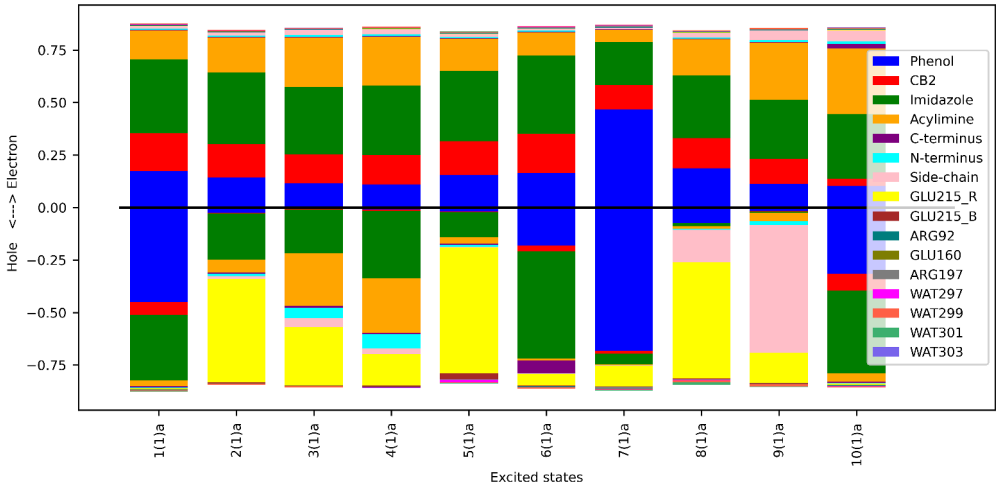

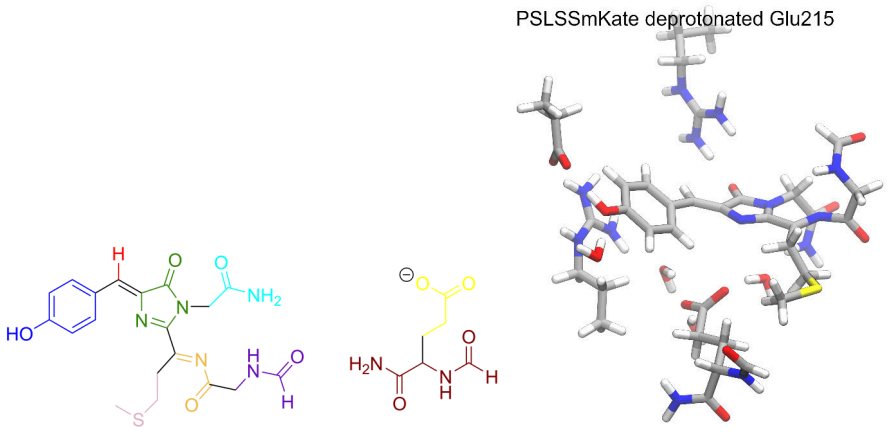

Figure S42: Fragment decomposition performed with TheoDORE of electron and hole populations of excited states of PSLSSmKate with deprotonated Glu215 calculated with CC2/def2-TZVP. Vertical excitation energies and oscillator strengths of each state are shown on the top. The QM region used in excited-state calculations and fragments corresponding to the chromophore and Glu215 are shown below, with colors matching those used in the plot.

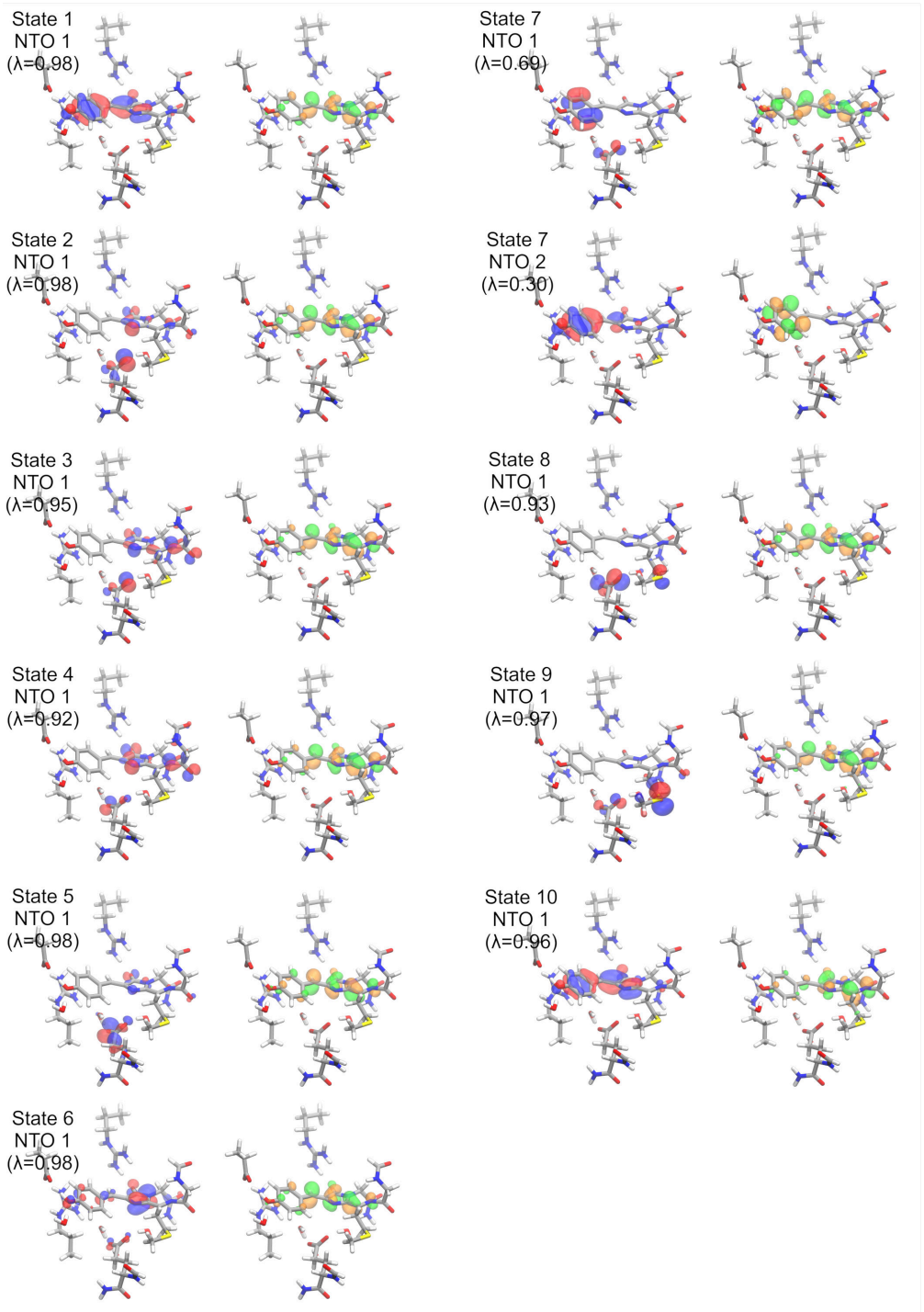

Figure S43: Most significant hole (red, blue) and electron (orange, green) NTOs of PSLSSmKate (deprotonated Glu215) excited states, calculated with RVS-CC2/def2-TZVP, corresponding to Figure S42.

State	$\Delta E(S_0 \rightarrow S_n)$/eV	f
1	3.250	0.940
2	3.992	0.016
3	4.170	0.003
4	4.309	0.002
5	4.454	0.003
6	4.525	0.021
7	4.556	0.001
8	4.617	0.000
9	4.839	0.001
10	5.020	0.106
11	5.163	0.016
12	5.214	0.007
13	5.259	0.125
14	5.457	0.007
15	5.511	0.012
16	5.541	0.011
17	5.568	0.000
18	5.604	0.010
19	5.632	0.009
20	5.637	0.005
21	5.705	0.003
22	5.766	0.214
23	5.874	0.000
24	5.885	0.011
25	5.905	0.007

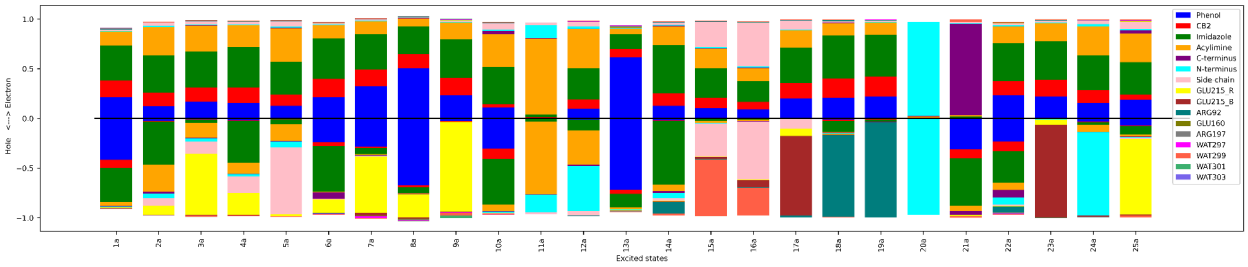

Figure S44: Fragment decomposition performed with TheoDORE of electron and hole populations of excited states of PSLSSmKate with deprotonated Glu215 calculated with CAM-B3LYP/def2-TZVP. Vertical excitation energies and oscillator strengths of each state are shown on the top. The QM region used in excited-state calculations and fragments corresponding to the chromophore and Glu215 are shown in Figure S42.

References

(1) Henderson, J. N.; Gepshtein, R.; Heenan, J. R.; Kallio, K.; Huppert, D.; Remington, S. J. Structure and Mechanism of the Photoactivatable Green Fluorescent Protein. *Journal of the American Chemical Society* **2009**, *131*, 4176–4177.

(2) Pletnev, S.; Shcherbakova, D. M.; Subach, O. M.; Pletneva, N. V.; Malashkevich, V. N.; Almo, S. C.; Dauter, Z.; Verkhusha, V. V. Orange Fluorescent Proteins: Structural Studies of LSSmOrange, PSmOrange and PSmOrange2. *PLOS ONE* **2014**, *9*, e99136.

(3) Royant, A.; Noirclerc-Savoye, M. Stabilizing role of glutamic acid 222 in the structure of Enhanced Green Fluorescent Protein. *Journal of Structural Biology* **2011**, *174*, 385–390.

(4) Tubbs, J. L.; Tainer, J. A.; Getzoff, E. D. Crystallographic Structures of Discosoma Red Fluorescent Protein with Immature and Mature Chromophores: Linking Peptide Bond Trans-Cis Isomerization and Acylimine Formation in Chromophore Maturation,. *Biochemistry* **2005**, *44*, 9833–9840.

(5) Piatkevich, K. D.; Malashkevich, V. N.; Almo, S. C.; Verkhusha, V. V. Engineering ESPT Pathways Based on Structural Analysis of LSSmKate Red Fluorescent Proteins with Large Stokes Shift. *Journal of the American Chemical Society* **2010**, *132*, 10762–10770.

(6) Piatkevich, K. D.; English, B. P.; Malashkevich, V. N.; Xiao, H.; Almo, S. C.; Singer, R. H.; Verkhusha, V. V. Photoswitchable Red Fluorescent Protein with a Large Stokes Shift. *Chemistry & Biology* **2014**, *21*, 1402–1414.